Satellite Observed Sensitivity of Tropical Clouds and Moisture to Sea Surface Temperature on Various Time and Space Scales: Part 1. Focus on High Level Cloud Situations over Ocean

Erik Höjgard-olsen, Hélène Chepfer, Hélène Brogniez

JGR Atmospheres

RESEARCH ARTICLE
10.1029/2021JD035438

This article is a companion to Höjgård-Olsen et al. (2022), https://doi.org/10.1029/2021JD035402

Key Points:

- The altitude of high clouds increases with sea surface temperature (SST) in observations over a range of space and time scales
- The opaque high cloud cover and middle-tropospheric relative humidity peak over SSTs of 302 K in the observations
- A global model reproduces the observed sensitivity of cloud altitudes to SST, but not the cloud opacity

Supporting Information:

Supporting Information may be found in the online version of this article.

Correspondence to:

E. Höjgård-Olsen,
erik.hojgard-olsen@latmos.ipsl.fr

Citation:

Höjgård-Olsen, E., Chepfer, H., & Brogniez, H. (2022). Satellite observed sensitivity of tropical clouds and moisture to sea surface temperature on various time and space scales: 1. Focus on high level cloud situations over ocean. *Journal of Geophysical Research: Atmospheres*, *127*, e2021JD035438. https://doi.org/10.1029/2021JD035438

Received 18 JUN 2021
Accepted 21 JAN 2022

Satellite Observed Sensitivity of Tropical Clouds and Moisture to Sea Surface Temperature on Various Time and Space Scales: 1. Focus on High Level Cloud Situations Over Ocean

Erik Höjgård-Olsen[1,2], Hélène Chepfer[1], and Hélène Brogniez[2]

[1]LMD/IPSL, Sorbonne Université, École Polytechnique, CNRS, Palaiseau, France, [2]LATMOS/IPSL, Université de Versailles Saint-Quentin-en-Yvelines, CNRS, Guyancourt, France

Abstract This study examines variations in high cloud properties and relative humidity (RH) with sea surface temperature (SST) over tropical oceans (30°N–30°S) using spaceborne lidar and microwave radiometer observations. The mean values over the tropics indicate that middle-tropospheric RH increases, high cloud covers decrease and cloud altitudes rise with SST. These signatures are consistent with the hypotheses proposed in the literature. The analysis of this same data set but at the scale of local processes shows different behaviors for SSTs <302 K and SSTs >302 K. Between 299 and 302 K, middle-tropospheric RH, opaque cloud cover, and cloud top altitude increase together with SST, while optically thin cloud cover decreases. Over SSTs >302 K, middle-tropospheric RH, opaque cloud cover, and opaque cloud top altitude decrease with SST, while the cover of optically thin clouds increases. Interestingly, the altitude of high clouds (not the cloud top) increases monotonically with SST from 299 to 305 K on a range of space and time scales, and the altitude of optically thin clouds remains higher than that of opaque clouds. The observed relationships on different time and space scales are compared to simulations of a global atmospheric model. Despite systematic biases, the model reproduces the sensitivity of the middle-tropospheric RH and cloud altitude to SST rather well but fails to reproduce the variations of the balance between high opaque cloud cover and high optically thin cloud cover.

Plain Language Summary High tropical clouds both cool and warm the planet by simultaneously reflecting incoming solar radiation and trapping energy that would have been emitted to space in cloud-free skies. It is unclear how these clouds will evolve when the climate warms. We use satellite observations over the tropical oceans and find that tropical mean variations show that the high clouds associated with thunderstorms rise and stay at about the same temperature, while their horizontal extent decrease. On the short and small scales where cloud and moisture processes occur, we find however that these high clouds become more opaque to radiation with sea surface temperature (SST) when it is colder than 302 K, and less opaque to radiation over waters warmer than 302 K. Simultaneously, the temperature of these clouds slightly decreases when they rise. Because models are the only tool to predict future climate change, we then compare the observed results to a global atmospheric model. The model reproduces roughly the observed middle-tropospheric humidity and cloud altitude variations but fails to reproduce the observed moisture variations in the lower and upper part of the troposphere, as well as the evolution of the opaque and thin high cloud covers with SST.

1. Introduction

Clouds and moisture are essential for the local and global climate, yet their responses to global warming are still not fully understood (Caldwell et al., 2016; Ceppi et al., 2017; Zelinka et al., 2020). Low clouds cool the climate, whilst high clouds have both cooling and warming effects. Sherwood et al. (2020) found the total uncertainty of cloud responses to global warming to be large, with comparable amounts accredited to high and low clouds. Thus, we have dedicated two companion articles to separately analyze observed variations of cloud properties and relative humidity (RH) with sea surface temperature (SST) in tropical (30°N–30°S) high and low cloud situations. This article (Part I) focuses on ***tropical high cloud situations***.

Several hypotheses have been proposed to anticipate how tropical high cloud regions are affected by warmer SSTs: high cloud cover has been hypothesized to decrease with SST due to increased convective precipitation efficiency that leaves fewer hydrometeors to build the convective anvils (*Iris* hypothesis; Lindzen & Choi, 2021; Lindzen et al., 2001). Meanwhile, the altitude of anvil detrainment is controlled by clear-sky mass convergence, which is a function of pressure, temperature, stability, and clear-sky radiative cooling rate. Because the latter is

constrained by Clausius-Clapeyron, the temperature at which it drops and the altitude of anvil detrainment are hypothesized to be invariant with surface temperature (*Fixed-Anvil Temperature*, FAT, hypothesis; Hartmann & Larson, 2002). Still, Zelinka and Hartmann (2010) found that anvils may warm slightly due to increased upper-tropospheric static stability (*Proportionally Higher-Anvil Temperature*, PHAT). Moreover, the increased upper-tropospheric stability may reduce the radiatively driven clear-sky mass convergence at the anvil height, weaken the convective detrainment, and reduce the anvil cover (*Stability Iris*; Bony et al., 2016).

After multiple reviews (e.g., Del Genio & Kovari, 2002; R. L. Li et al., 2019; Lin et al., 2002, 2004; Mauritsen & Stevens, 2015; Rapp et al., 2005; Seeley et al., 2019; Yoshimori et al., 2020), the essences of these hypotheses have survived in current climate models (e.g., Ceppi & Gregory, 2017; Dessler, 2010; Vial et al., 2013; Zelinka et al., 2016, 2017), that suggest a warming by decreasing anvil cloud cover and reduced shortwave reflection and cooling by less longwave trapping. Simultaneously, they suggest a warming by rising altitudes of convective anvils that keep their emission temperatures independent of surface temperature.

In observations, variations of tropical high cloud properties with SST differ in both sign and magnitude, depending on the observed cloud parameter, scale, and region. Tropical high cloud cover responses to SST warming varies most substantially, from −13 to +13%/K (Behrangi et al., 2012; Choi et al., 2017; Hartmann & Michelsen, 2002; Höjgård-Olsen et al., 2020; Su et al., 2008, 2017), whilst rising tropical high cloud altitudes with SST warming has been observed on all scales (Igel et al., 2014; Y. Li et al., 2012; Norris et al., 2016; Zhou et al., 2014), although with varying responses of cloud emission temperature (Eitzen et al., 2009; Thompson et al., 2017; Xu et al., 2007; Zelinka & Hartmann, 2011).

The time and space scales evidently matter for high cloud responses to SST warming. The instantaneous local view is close to the fast and small scales where cloud processes occur, and the annual global mean view is tied to climate sensitivity. However, different processes and mechanisms prevail on different temporal and spatial scales (Forster et al., 2016; Klein et al., 2017; Orlanski, 1975; Steyn et al., 1981). Thus, Sherwood et al. (2020) raised concerns about cloud responses to variations of surface temperature on short and local scales and how they are tied to the long-term global climate.

In this study, we investigate the responses of high cloud situations from an observational perspective, to understand:

1. How do tropical high cloud properties (cover, altitude, temperature) and RH profiles vary with SST?
2. Which physical mechanism dominates the observed signal on both the process and annual tropical mean scale?
3. Under which specific conditions are the hypothesized literature mechanisms described above valid?
4. How are the observed physical relationships reproduced by a general circulation model?

Section 2 describes the satellite data that are used: high clouds observed by the Cloud-Aerosol Lidar and Infrared Pathfinder Satellite Observation (CALIPSO; Winker et al., 2009) and RH profiles observed by the Sounder for Atmospheric Profiling of Humidity in the Intertropics by Radiometry (SAPHIR; Roca et al., 2015). Section 3 presents the method to establish co-variations between high clouds, RH profiles and SST on instantaneous, monthly, and annual timescales at local scale and averaged over the tropical oceans. Section 4 describes the variables' mean states. In Section 5, we analyze the responses of cloud cover, altitude, and RH to SST separately; first from an observational perspective, then with model simulations. Since most recent studies on FAT and Iris are heavily model-based, it is useful to confront this model-based view with an advanced observational analysis (Lindzen & Choi, 2021). In Section 6, we tie these individual variable responses together considering the hypotheses described above. Section 7 contains the main conclusions.

2. Data

We use once daily (01:30 p.m. local time - LT) data of cloud properties, RH and SST collected over tropical oceans (30°N–30°S). The individual data sets cover different periods, but comparisons with results obtained over the overlapping period (2012–2018) show that our main conclusions are insensitive to time period. Therefore, we perform the analyses over the longest available period for each observational data set.

2.1. Observations of Cloud Properties

We use cloud observations from the 1° × 1° gridded General Circulation Model-Oriented CALIPSO (Winker et al., 2009) Cloud Product V3.1.2 (Chepfer et al., 2010; Guzman et al., 2017). We distinguish clouds by opacity: Opaque clouds (e.g., deep convective clouds) have optical depths >3–5 depending on the cloud microphysics and are characterized by full attenuation of the lidar beam. Thin clouds (e.g., cirrus) have optical depths <3–5 and the lidar detects a surface echo. We use opaque/thin cloud covers (C_{OPAQUE}, C_{THIN}), altitudes (Z_{OPAQUE}, $Z_{\mathrm{OPAQUE,TOP}}$, Z_{THIN}) and temperatures ($T_{Z_{\mathrm{OPAQUE}}}$, $T_{\mathrm{OPAQUE,TOP}}$, T_{OPAQUE}, T_{THIN}). Following Vaillant de Guélis et al. (2017), Z_{OPAQUE} is the altitude where the satellite lidar beam becomes fully attenuated, $Z_{\mathrm{OPAQUE,TOP}}$ the altitude of opaque cloud top, and Z_{THIN} the altitude half-way between thin cloud top and base. The temperatures at these altitudes are $T_{Z_{\mathrm{OPAQUE}}}$, $T_{\mathrm{OPAQUE,TOP}}$, and T_{THIN}. Moreover T_{OPAQUE} is the temperature at the opaque cloud altitude half-way between Z_{OPAQUE} and $Z_{\mathrm{OPAQUE,TOP}}$, which drives the outgoing longwave radiation (Vaillant de Guélis et al., 2017). GOCCP data is available from April 2006, but we use the period 2008–2019 because the lidar's direction of pointing was tilted slightly in 2007, which affected the homogeneity of the cloud property retrievals. We show only the daytime measurements (01:30 p.m. LT) to be consistent with the data set built in Höjgård-Olsen et al. (2020) that also included CloudSat observations which are only available during daytime since 2011.

2.2. Observations of Atmospheric RH

We analyze RH observations (defined with respect to liquid water, Sivira et al., 2015) from the 1° × 1° gridded L2B product derived from the SAPHIR radiometer onboard Megha-Tropiques that measures upwelling brightness temperatures in six channels centered around the 183.31 GHz water vapor absorption line (Roca et al., 2015; Sivira et al., 2015). The swath of SAPHIR is 1,700 km with a nominal footprint resolution of 10 km at nadir (Brogniez et al., 2013; Eymard et al., 2002). RH profiles are derived from SAPHIR measurements over six atmospheric layers over 100–950 hPa (Brogniez et al., 2016; Sivira et al., 2015). We use three layers to represent RH in the lower- (950–850 hPa), middle- (600–400 hPa), and upper (200–100 hPa) troposphere (LTRH, MTRH, UTRH, respectively). SAPHIR L2B data is available from October 2011, but due to technical issues late in 2018, we only consider the 2012–2018 period. Moreover, we use observations at 01:30 p.m. LT to be consistent with the cloud properties.

2.3. SST From Reanalysis

We use SST from the fifth generation of the ECMWF reanalysis (ERA5; Dee et al., 2011; Hoffmann et al., 2018). We take once daily values at 01:30 p.m. LT as the average value of the 01:00 p.m. and 02:00 p.m. SSTs. This reanalysis product is of appreciable accuracy for our work, as SST is a slowly varying parameter (although with a small diurnal cycle in convective regions, typically ±0.6 K; Bellenger & Duvel, 2009; Hughes et al., 2020) and widely used in the community.

2.4. IPSL-CM6 General Circulation Model

Finally, we consider two sets of climate model simulations from the IPSL-CM6 (Institut Pierre Simon Laplace-Coupled Model v6; Hourdin et al., 2006, 2020) model. The model runs on a 1.27° × 2.5° grid, and we analyze the three hourly simulations for the Atmospheric Model Intercomparison Project configuration ("AMIP", Ackerley et al., 2018), in which the GCM is run with prescribed time-varying SSTs and sea ice concentrations from observations and includes variations in natural and anthropogenic external forcing. We refer to this first simulation (the AMIP run) as "current climate". The second simulation is the corresponding AMIP + 4 K simulation (referred to as "warmer climate"), where the SST has been uniformly increased by +4 K (Ackerley et al., 2018). Both AMIP and AMIP + 4 K runs are analyzed over the 2006–2014 period which overlaps the CALIPSO/CloudSat observational record. We extract the 01:30 p.m. LT time step to be consistent with the observations.

We use the same variables as in the observational data sets (RH profiles, cloud properties, SST) for the AMIP/AMIP + 4 K simulations. Cloud properties are simulated with the CFMIP (Cloud Feedback Model Intercomparison Project) Observation Simulator Package version 2 (COSP2; Bodas-Salcedo et al., 2011; Swales et al., 2018) lidar simulator (Chepfer et al., 2008; Guzman et al., 2017), which mimics the clouds that would have been

observed by the CALIPSO lidar, had it flown over the modeled atmosphere. RH is taken from seven available atmospheric pressure levels in the AMIP/AMIP + 4 K simulations ranging over 850–10 hPa. Thus, simulated LTRH, MTRH, and UTRH are considered at 850, 500, and 150, respectively.

3. Collocation Method and Trend Analysis

3.1. Collocation

We use two methods to collocate observations of cloud properties and RH. These are described next and illustrated by the flowchart in Figure S1 in Supporting Information S1.

3.1.1. Instantaneous Collocation Method

We collocate gridded orbit files of cloud and RH data on the instantaneous scale (01:30 p.m. LT). We allow the SAPHIR measurements a 2 hr window around 01:30 p.m. for collocation with CALIPSO and ERA5 on the 1° × 1° grid box scale. A high cloud data set is extracted by only keeping grid boxes where SST ≥299 K, and cloud temperatures $T_{Z_{OPAQUE}}$ ≤240 K or T_{THIN} ≤240 K. SST ≥299 K is a reasonable approximation for the onset of tropical deep convection (hereafter "DC", Aumann et al., 2017; Evans & Webster, 2014; N. C. Johnson & Xie, 2010), and cloud temperatures ≤240 K target the bottom of the anvil detrainment region in the coldest clouds (Kuang & Hartmann, 2007; Luo et al., 2012). These *local instantaneous values* represent the processes at play. From these local instantaneous values, we compute local monthly mean 1° × 1° maps, as well as monthly and annual spatial averages over tropical oceans. The latter are weighted averages referred to as *tropical mean values* that reflect climatic-scale states. Thus, we have a first package of 4 different tropical high cloud data sets: 2 for the local grid box scale (instantaneous; monthly), and 2 for the tropical mean scale (monthly; annual).

3.1.2. Timescale Collocated Method

We compute monthly and annual values for each variable and every 1° × 1° grid box, independently of the other variables. The criteria of SST ≥299 K and $T_{Z_{OPAQUE}}$ ≤240 K or T_{THIN} ≤240 K are then applied to the monthly and annual timescales. In this method, we perform the spatial collocation after the initial temporal upscaling to obtain the tropical mean values. Hereafter we use a second package of 2 different tropical mean high cloud data sets (monthly; annual).

Figure 1a shows the occurrence of the high cloud (SST ≥ 299 K and $T \leq 240$ K) data set in the all-cloud data set (containing any cloud). High clouds are observed in convective regions, where they occur in 40%–60% of the all-cloud data set. This data set is dominated by high thin clouds (Figure 1c), due to the typically colder T_{THIN} (higher Z_{THIN}) than $T_{Z_{OPAQUE}}$ (lower Z_{OPAQUE}). These coldest high opaque clouds (Figures 1b and 1d) occur in 5%–10% of the all-cloud data set and only in deep convective regions.

3.2. Method to Characterize Co-Variations

Figure 2 shows how high opaque cloud altitude (Z_{OPAQUE}) varies with SST over the 2008–2019 period, on the local (a, b) and tropical mean scales (c).

On the local scale (Figures 2a and 2b), we use the median (black line) Z_{OPAQUE} value in each SST bin to account for possible nonlinearities. As in Höjgård-Olsen et al. (2020), median values are computed for each 0.25 K SST bin of minimum five available values. A bootstrapping algorithm (500 random samplings with replacement) then removes non-significant median values that lie outside of the 90% confidence interval. Additionally, median values computed from less than 100 values are highlighted by gray areas (Figures 2a and 2b).

Unlike the local view (1° × 1° scale), tropical means are spatially averaged values, meaning that the relationship between Z_{OPAQUE} and SST on the tropical mean scale are either weighted toward the cloud population most frequently observed, or toward the cloud population most sensitive to SST. Therefore, interannual variations on the tropical mean scale typically reflect one of those populations.

On this tropical mean scale, the relationship between Z_{OPAQUE} and SST can be represented with a linear regression fit (Figure 2c). We compute linear regressions using orthogonal distance regression (ODR, Boggs et al., 1992; Boggs & Rogers, 1990; Boggs et al., 1988) that accounts for measurement errors in both variables by seeking the smallest orthogonal difference between each observation and the linear fit. We prefer ODR when we observe

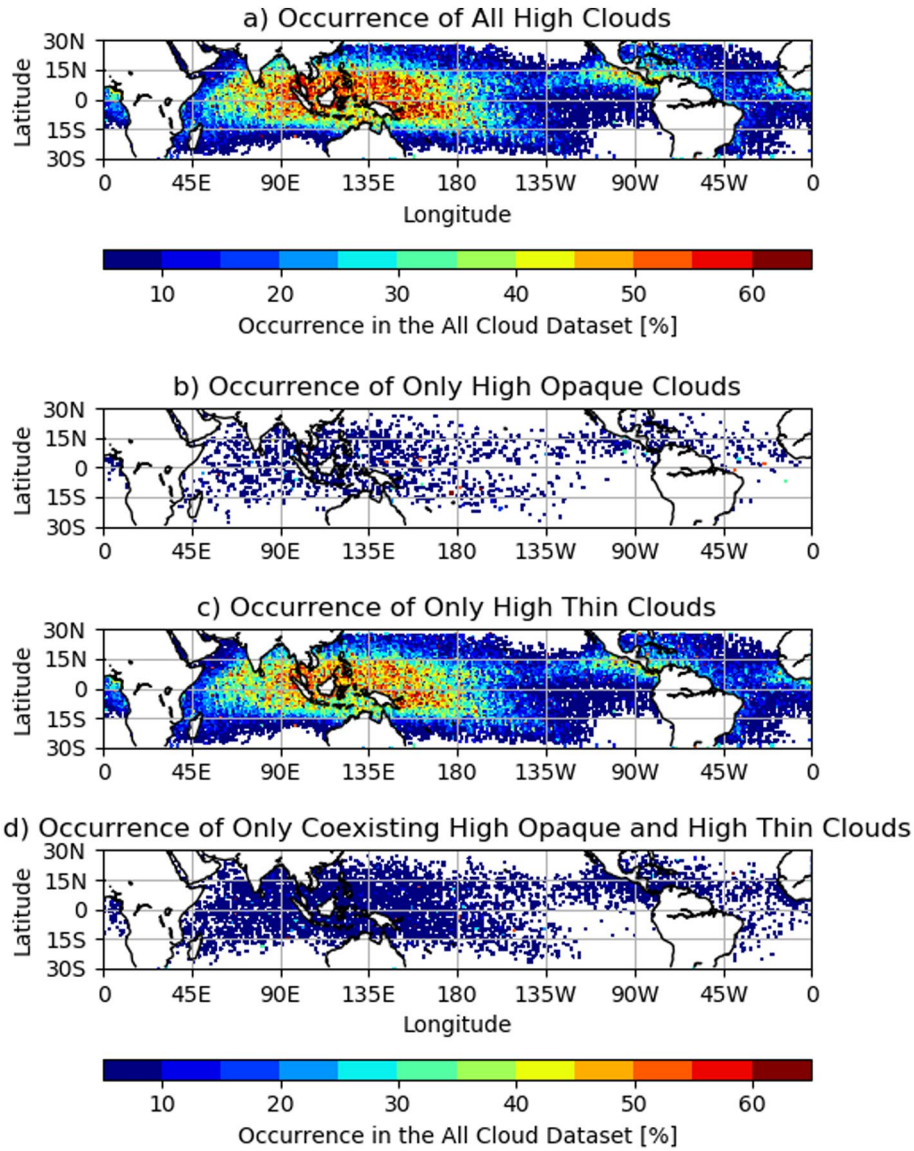

Figure 1. Occurrence of only (a) high clouds, (b) high opaque clouds, (c) high thin clouds, (d) coexisting high opaque and thin clouds, with respect to All Clouds. In (a) the occurrence is the number of $1° \times 1°$ grid boxes containing high clouds (cloud cover > 0%, SST $\geq$ 299 K, $T \leq 240$ K) divided by the number of $1° \times 1°$ grid boxes containing clouds (cloud cover > 0%). Therefore $a = b + c + d$. Opaque and thin clouds are separated by optical depth based on the capability of the lidar to detect the surface echo. Opaque clouds typically correspond to an optical depth >3–5 while thin clouds correspond to smaller optical depths. White color means no grid boxes containing tropical oceanic high clouds.

snapshots of the atmosphere and cannot be sure that one variable is measured without error (Leng et al., 2007; Lolli & Gasperini, 2012). Finally, we assess statistical significance of the linear regressions with a p-value $\leq$0.05 (Fisher, 1956).

Monthly mean values are often used in the literature, but studies of co-variations based on this timescale mix changes in clouds and SST patterns with seasonal variability and might thus be more difficult to interpret physically than values retrieved from instantaneous and annual.

The two following statements remain true for all variables used in this study: (a) Linear regressions are good representations of tropical mean variations with SST, whilst often not for nonlinear local variations. (b) We observe similar variations with SST for the same variable on the monthly and instantaneous local (grid box) scales. Hereafter, we use monthly and instantaneous medians (Figures 2a and 2b) to describe the "process scale"

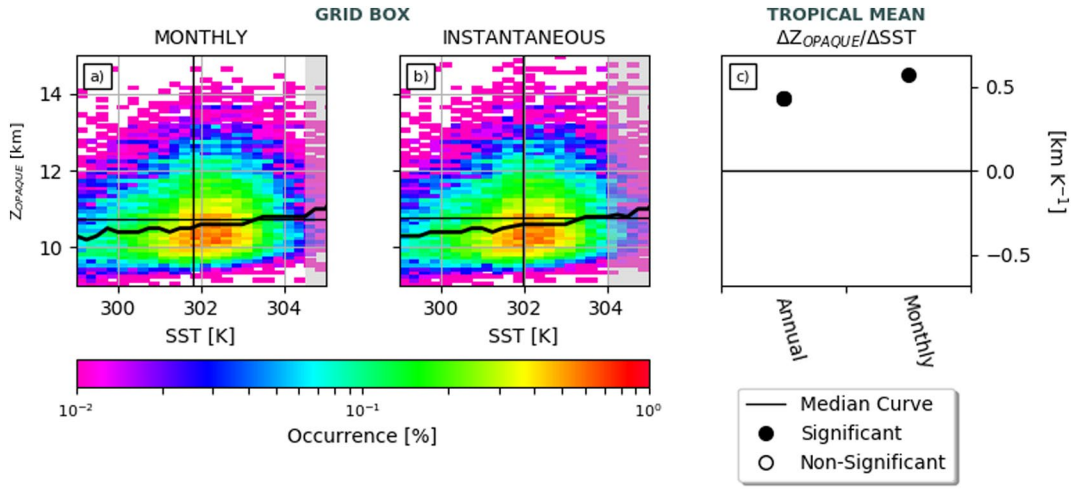

Figure 2. (a and b) Density scatter plots of grid box values of opaque cloud altitude versus sea surface temperature (SST) on the local monthly and instantaneous timescales over the years 2008–2019 computed with the *Instantaneous Collocation Method*. Black curves show the median value in each SST bin. Gray filters mask SST bins that contain less than 100 cloud altitude values. (c) Regression slopes between tropical mean Z_{OPAQUE} and tropical mean SST (see also Figure S6 in Supporting Information S1).

whilst annual and monthly slopes of linear regression fits (Figure 2c) to summarize the tropical mean rates of change.

4. Results for Mean States

Figure 3 shows the mean states of the observed variables in the high cloud data set. The patterns of high C_{OPAQUE} (Figure 3a), MTRH (Figure 3h), and SST (Figure 3j) look similar, due to DC: high opaque clouds occur mostly over SSTs >301 K (Figures 1b and 1d), where the MTRH is maximum (>40%, Figure 3h), $Z_{\mathrm{OPAQUE}} > 11$ km (Figure 3c), and $T_{Z_{\mathrm{OPAQUE}}} < 233$ K (Figure 3e).

The patterns of high thin clouds look like upper-tropospheric RH (UTRH; Figure 3g) and are less tied to SST than high opaque clouds because they include both cirrus formed by convective detrainment and those formed in situ away from detrainment regions.

Figure 4 is the same as Figure 3 but for the model current climate simulation. In the model, all variables exhibit similar spatial distributions as SST (Figure 4j). Hence, there is no distinction between patterns of opaque and thin cloud properties in the model, which seems to have difficulties to produce cirrus away from DC areas.

5. Results for Variations With SST

We first analyze how high cloud properties and RH vary with SST on different time and space scales in the observations, and then if the model reproduces the observed relationships.

5.1. Cloud Covers

5.1.1. Observed Variations With SST

Annual tropical means (Figure 5) show that both C_{OPAQUE} (−7.5%/K, Figure 5a) and C_{THIN} (−2.6%/K, Figure 5b) decrease with SST. The negative annual regressions are close between the two collocation methods (circles and triangles) for both C_{OPAQUE} (−7.3 and −7.5%/K, Figure 5a) and C_{THIN} (−2.6 and −2.7%/K, Figure 5b), which implies that interannual variations of tropical mean high cloud cover are robust to whether the data are collocated before or after time averaging.

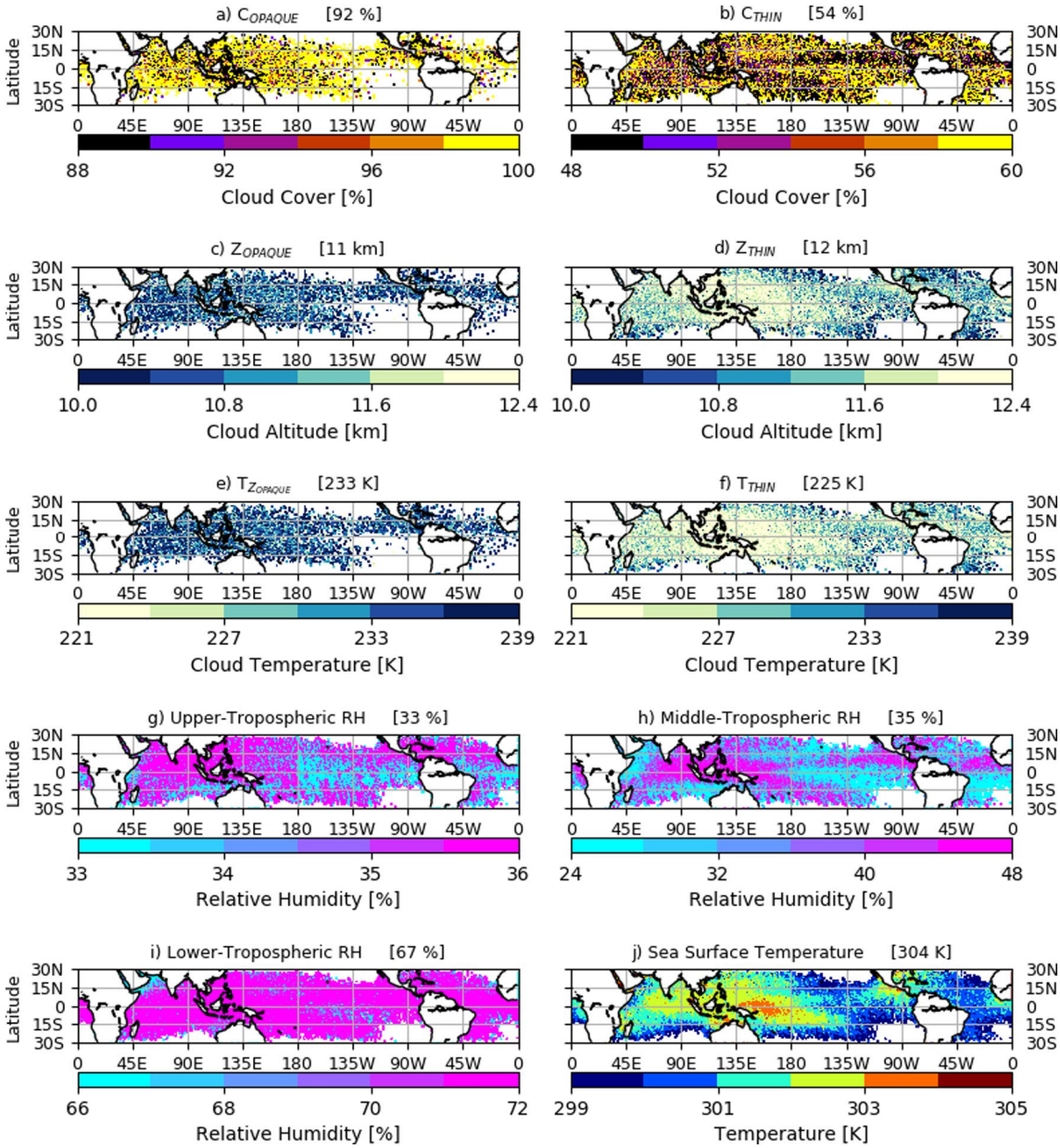

Figure 3. Observations in high cloud situations. C_{OPAQUE} (resp. C_{THIN}) is the average of C_{OPAQUE} (resp. C_{THIN}) values only in grid boxes containing opaque (resp. thin) high clouds (SST ≥ 299 K, $C_{\mathrm{OPAQUE}} > 0\%$, $T_{Z_{\mathrm{OPAQUE}}} \leq 240$ K, resp. SST ≥ 299 K, $C_{\mathrm{THIN}} > 0\%$, $T_{\mathrm{THIN}} \leq 240$ K). For subplots (g–j) values are averaged only over SSTs ≥ 299 K where $T_{\mathrm{THIN}} \leq 240$ K and/or $T_{Z_{\mathrm{OPAQUE}}} \leq 240$ K. Mean values computed with the Instantaneous collocation method.

The decrease in annual tropical mean C_{THIN} (−2.6%/K) is consistent with the annual −2%/K decrease in Saint-Lu et al. (2020) who used the same data set as in the current study (CALIPSO-GOCCP) and focused on thin clouds located at altitudes >8 km in monthly means.

Figure 6 shows the local cloud cover variations with SST. The decrease in tropical mean C_{OPAQUE} (Figure 5a) reflects the behavior of the local data located over deep convective SSTs (302–304 K) in Figure 6a but masks the behavior of the more numerous opaque clouds over SSTs 299–302 K. In contrast, the decrease in annual tropical mean C_{THIN} (Figure 5b) reflects the behavior of most of the population (299–302 K in Figure 6b and Figure S2d in Supporting Information S1), and not the behavior over SSTs >302 K (Figure 6b) that we associate with convective detrainment on the process scale.

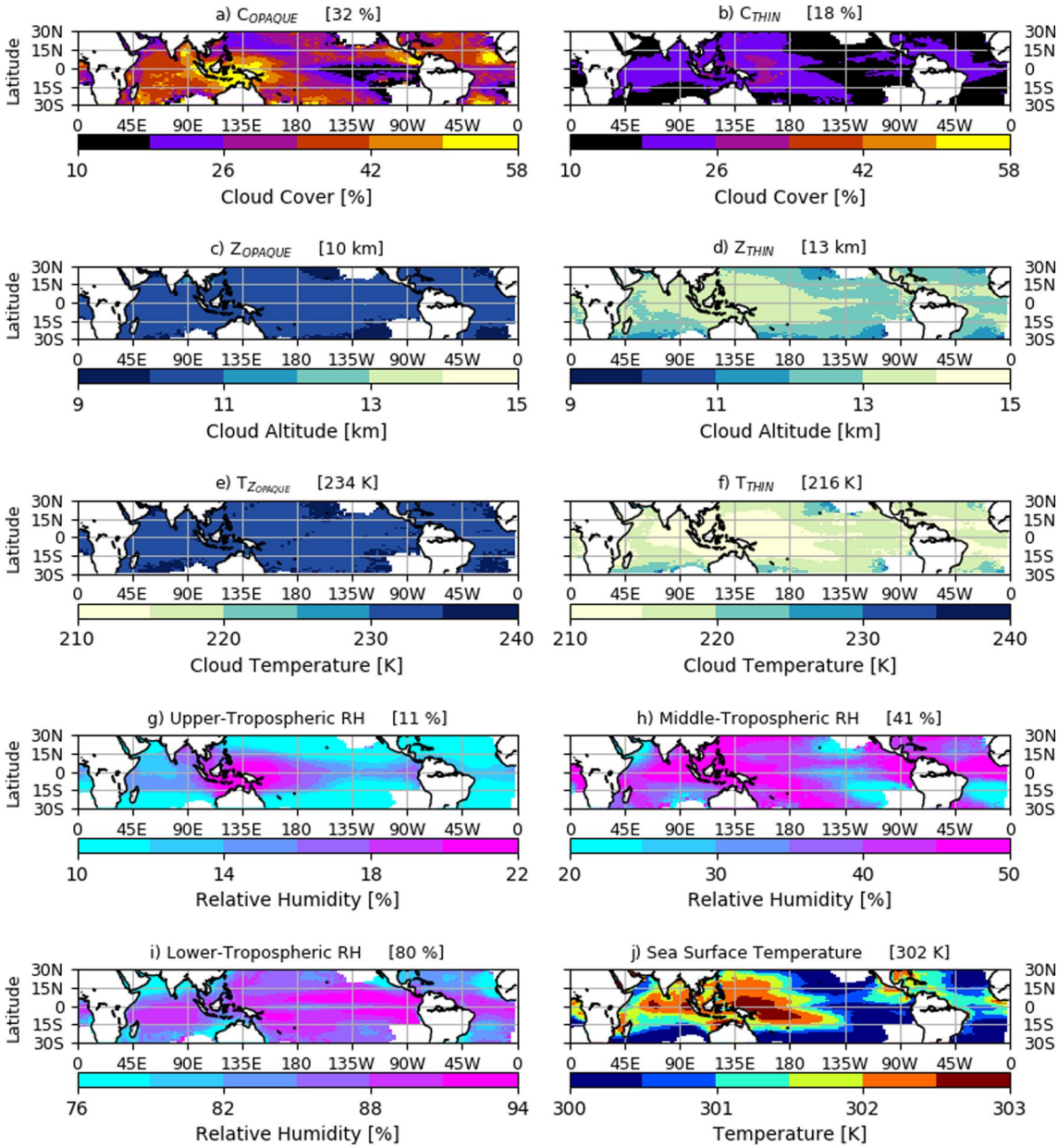

Figure 4. Same as Figure 3, but for the model current climate.

Local instantaneous observations (Figure 6, top panel, blue lines) show that tropical high cloud cover varies nonlinearly with SST on the process scale. C_{OPAQUE} is maximum (Figure 6a) at SST = 302 K, which corresponds to the maximum occurrence of DC (Houze et al., 2015; Sabin et al., 2013; Waliser et al., 1993). The strong nonlinear signal of C_{OPAQUE} on the instantaneous scale (Figure 6a) is smoothed out on the monthly scale (and even longer timescales), where the initial increase over SSTs <302 K is most affected, which explains why the multiannual mean C_{OPAQUE} (Figure 3a) does not bear resemblance to the underlying SST distribution (Figure 3j). The nonlinear variation of C_{OPAQUE} with SST (Figure 6a) is consistent with Behrangi et al. (2012; CloudSat 2B-CLDCLASS product; 2007–2008).

In contrast, C_{THIN} is weakly sensitive to SST (50%–60%) because many cirrus clouds are formed in situ away from DC (Luo & Rossow, 2004; Reverdy et al., 2012). However, C_{THIN} exhibits a slight signal of DC, as shown by a local minimum over SST = 302 K where the occurrence of DC is maximum. Interestingly, the variations of C_{OPAQUE} and C_{THIN}, in 1° × 1° grid boxes where high opaque and high thin clouds coexist, balance each

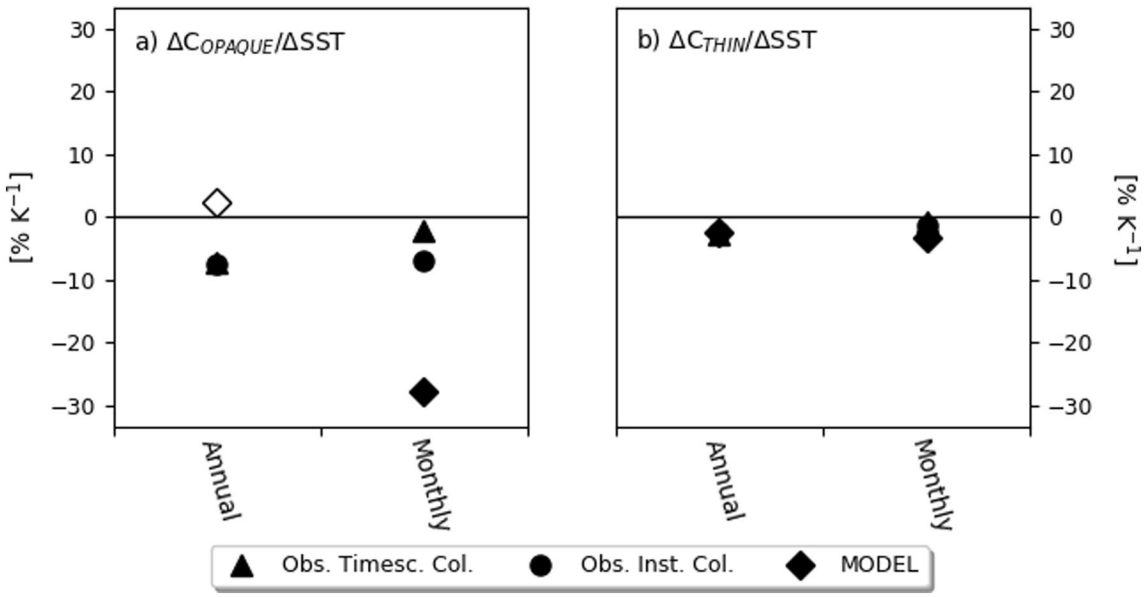

Figure 5. Slopes of linear regressions between cloud covers and sea surface temperature (SST), computed using tropical mean annual and monthly values (like Figure 2c) defined from observations (triangles and circles) and model values (lozenges). Left: C_{OPAQUE}. Right: C_{THIN}. Filled (empty) symbols represent significant (non-significant) values.

other to maintain the total high cloud cover >90% on the instantaneous local scale (Figure S5 in Supporting Information S1).

5.1.2. Model Variations With SST in Current Climate

Regarding C_{OPAQUE}, the model annual tropical mean variation (Figure 5a) does not agree with the observations, since the observations show a decrease, while the model does not reproduce this relationship. The magnitude of the monthly model regression (−27.7%/K) is extremely overestimated compared to observations. At local instantaneous scale (Figure 6c), modeled C_{OPAQUE} behaves roughly like the observations: C_{OPAQUE} peaks around the SSTs corresponding to the maximum occurrence of DC, but this peak is biased toward slightly too warm SSTs (303 K instead of 302 K). Moreover, C_{OPAQUE} is strongly underestimated by the model by a factor 2–4 over all SSTs (Perpina et al., 2021). This suggests that the mechanism to produce high opaque clouds through DC in the model is about right, but not efficient enough and occurs at 1 K too warm SST.

In contrast, the annual tropical mean regression for C_{THIN} (−2.4%/K, Figure 5b) is close to the observations (−2.6%/K), whilst at local instantaneous scale (Figure 6d), modeled C_{THIN} behaves opposite to the observations. Indeed, modeled C_{THIN} peaks at the maximum occurrence of DC (like modeled C_{OPAQUE}), whilst the observed C_{THIN} is minimum there, which suggests that the *relative* importance of the convective vs. non-convective generation of thin clouds is not well captured by the model.

Zelinka et al. (2013; 5 coupled atmosphere-ocean CMIP5 models) found locally decreasing annual ensemble-mean high thin cloud cover (about −1.5%/K), whilst no notable change in thick high cloud cover in Oceania. Although these model results are not directly comparable to our model results due to the different methodology, they are compatible with the annual regressions of high C_{OPAQUE} (nonsignificant) and C_{THIN} (−2.4%/K; Figure 5). Therefore, the model biases might be shared by other models.

5.1.3. Predicted Changes in a Warmer Climate

Figure 7 shows the difference between model-simulated mean states in the AMIP + 4 K climate compared to the current climate (AMIP). C_{OPAQUE} and C_{THIN} exhibit regional responses to this warming. However, tropical mean changes are very small (C_{OPAQUE}: 0%/4 K = 0%/K, Figure 7a, and C_{THIN}: −1%/4 K = −0.25%/K, Figure 7b), in strong contrast to the large model current climate variabilities in Figures 5a and 5b: −27.7%/K for monthly C_{OPAQUE} and −2.4%/K for annual C_{THIN}. For C_{THIN} the sign of current climate variability (negative, Figure 5b) is consistent with the sign of forced change in a warmer climate (Figure 7b), although the amplitude is much

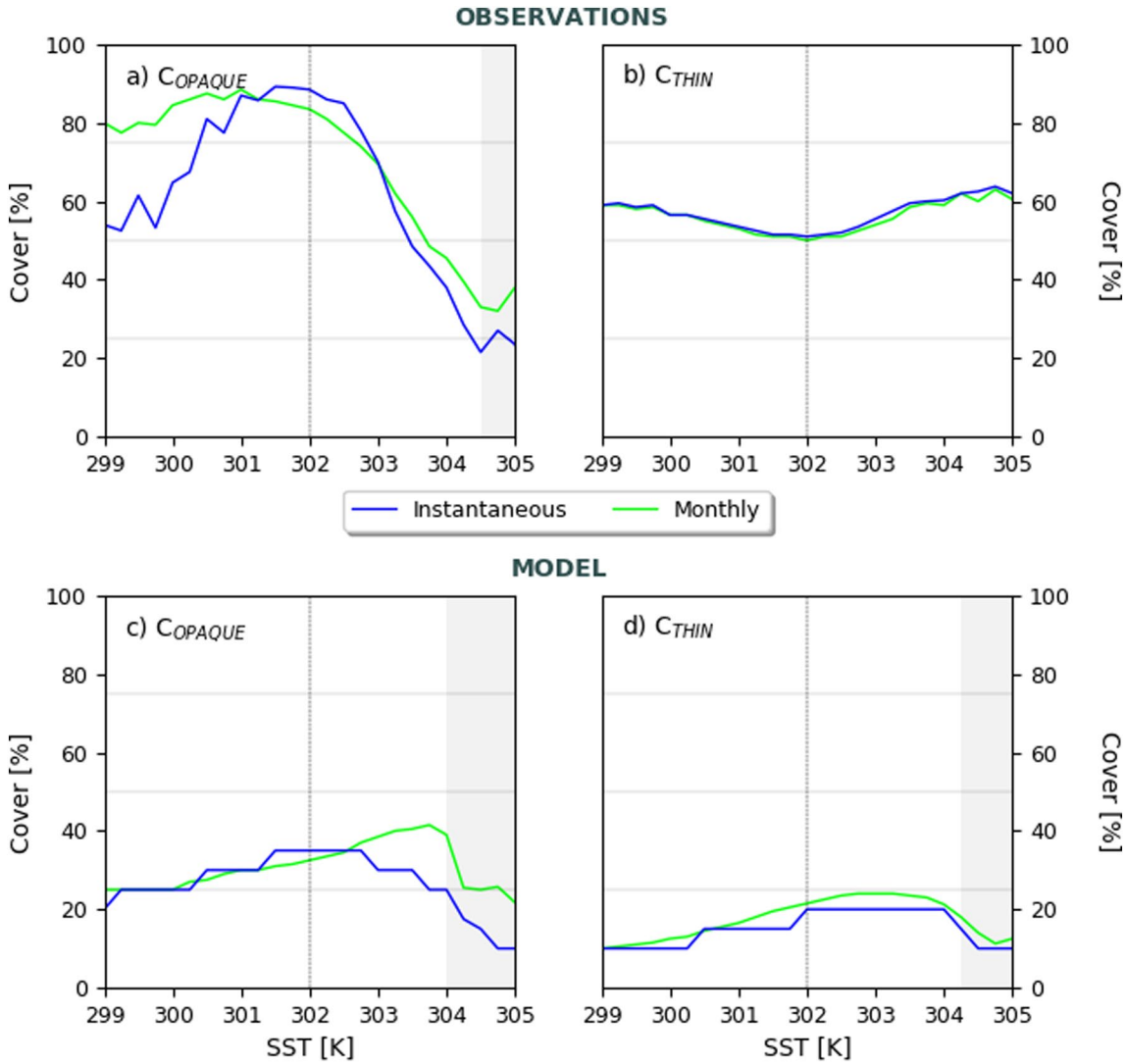

Figure 6. Variations of C_{OPAQUE} (left column) and C_{THIN} (right column) with SST computed using 1° × 1° data on the instantaneous (blue) and monthly (green) timescales (curves represent medians like Figures 2a and 2b). The vertical dotted line at SST = 302 K marks the maximum occurrence of deep convection.

smaller as previously identified for this model by Vaillant de Guélis et al. (2018) and for other models by Zhou et al. (2015).

Because the model does not reproduce the observed sensitivity of C_{OPAQUE} to SST on the tropical mean scale (Figure 5a), and only roughly reproduces this sensitivity locally (Figures 6a and 6c), the predicted response of C_{OPAQUE} to forced SST change (Figure 7a) is weakly reliable. The predicted response of C_{THIN} to forced SST change (Figure 7b) is also weakly reliable because at local scale (Figure 6b) the model does not reproduce the observed sensitivity of C_{THIN} to SST. Nevertheless, the large-scale circulation change is a confounding factor for analyzing the +4 K predictions (e.g., Perpina et al., 2021).

5.2. Cloud Altitudes

5.2.1. Observed Variations With SST

Annual tropical means (Figure 8) show that both Z_{OPAQUE} (+0.43 and +0.57 km/K, Figure 8a) and Z_{THIN} rise (+0.34 and +0.57 km/K, Figure 8b) in both collocation methods. The rise of Z_{THIN} (+0.34 km/K) is consistent with +0.3 km/K in Saint-Lu et al. (2020). These tropics-wide altitude changes (Figure 8) reflect the process scale (Figure 9).

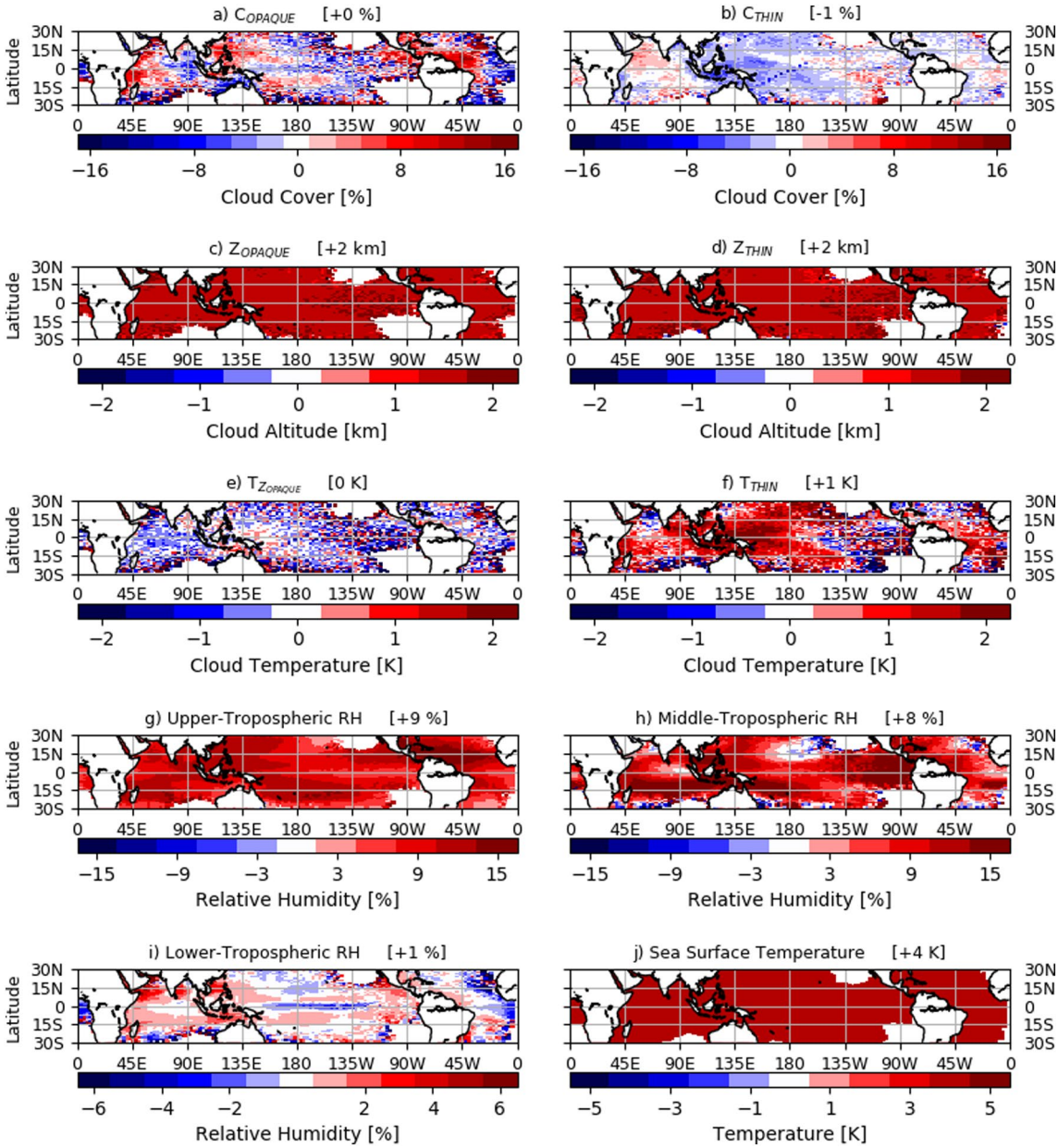

Figure 7. Absolute difference between the model warmer climate (AMIP + 4 K) and current climate (AMIP) simulations. Values in brackets are the tropical mean differences.

Local instantaneous observations (Figure 9, top panel, blue lines) show that both Z_{OPAQUE} and Z_{THIN} rise approximately linearly with SST by +0.13 and +0.21 km/K respectively (Figures 9a and 9b), The cloud temperatures $T_{Z_{\mathrm{OPAQUE}}}$ and T_{THIN} cool by −0.7 and −1.2 K/K (Figures S4a and S4b in Supporting Information S1). Interestingly, the cloud top altitude $Z_{\mathrm{OPAQUE,TOP}}$ (dashed curves) decreases slightly over SSTs 303–305 K and the opaque cloud top temperature $T_{\mathrm{OPAQUE,TOP}}$ warms by +1.5 K/K (Figure S4a in Supporting Information S1) there. That the distance between Z_{OPAQUE} and $Z_{\mathrm{OPAQUE,TOP}}$ decreases over SSTs >302 K implies that the lidar attenuation is happening faster and that the mean ice water content increases there.

5.2.2. Model Variations With SST in Current Climate

Model annual tropical means (Figure 8, lozenges) Z_{OPAQUE} (+0.56 km/K, Figure 8a) and Z_{THIN} (+0.58 km/K, Figure 8b) increase with SST, consistently with the observations. The model increases in tropical means (Figures 8a and 8b) reflect the model local scale variations with SST (Figures 9c and 9d).

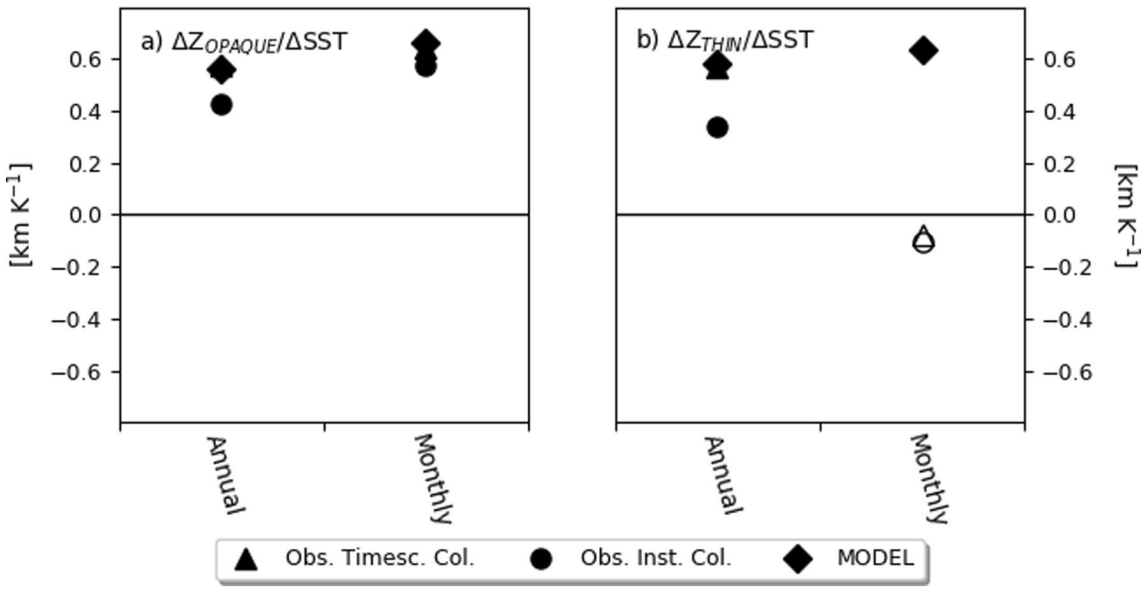

Figure 8. Same as Figure 5, but for cloud altitudes ΔZX/ΔSST. Left: Z_{OPAQUE}. Right: Z_{THIN}.

Local instantaneous simulations (Figure 9, bottom panel, blue lines) show that modeled Z_{OPAQUE} (Figure 9c) and Z_{THIN} (Figure 9d) rise more rapidly than the observed over SSTs 299–301.5 K and settle at plateau values, but decrease again over the non-significant SSTs (gray area). In contrast to the observations, the model simulates similar fluctuations of Z_{OPAQUE} and $Z_{OPAQUE,TOP}$ with SST.

The increases in our modeled Z_{OPAQUE} (Figure 8c) and Z_{THIN} (Figure 8d) with SST are ∼2 times larger in magnitude than Zelinka et al. (2013) who found decreasing ensemble mean cloud top pressure (−30 hPa/K, about +0.25 km/K in a hydrostatic atmosphere) with global warming along the ITCZ.

5.2.3. Predicted Change in a Warmer Climate

Figure 7 shows rising tropical-mean Z_{OPAQUE} and Z_{THIN} (+2 km/4 K = +0.5 km/K) and warming T_{THIN} (+1 K), whilst no change in $T_{Z_{OPAQUE}}$. This +0.5 km/K average rise-up of Z_{OPAQUE} and Z_{THIN} attributable to the +4 K warming is close to the sensitivities of Z_{OPAQUE} and Z_{THIN} to SST in current climate simulations and observations (Figures 8a and 8b).

Moreover, this response is also consistent with previous studies, such as a +0.42 km/K rise in tropical opaque and thin cloud fraction profiles in a +4 K climate scenario in Chepfer et al. (2014), and about +0.25 km/K with global warming in Zelinka et al. (2013). Additionally, the +1 to +2 K warming of T_{THIN} (Figure 7f) is consistent with Thompson et al. (2017) who found the temperature at the altitude of maximum tropical cloud fraction to warm by +3 K in the AMIP +4 K scenario.

We have high confidence in future predictions of cloud altitudes, because the model reproduces the observed sensitivities to SST in the current climate, on both the local (Figure 9) and tropical mean scales (Figure 8), and because rising altitudes are consistent with the predicted cloud altitude response to a +4 K SST forcing (Figure 7). Moreover, the model predictions are also consistent with the FAT and PHAT theories.

5.3. Relative Humidity

5.3.1. Observed Variations With SST

Annual tropical means (Figure 10) indicate that UTRH increases with SST in both collocation methods (+3.6 and +2.5%/K, Figure 10c), without significant change in MTRH (Figure 10b). The increasing tropical mean

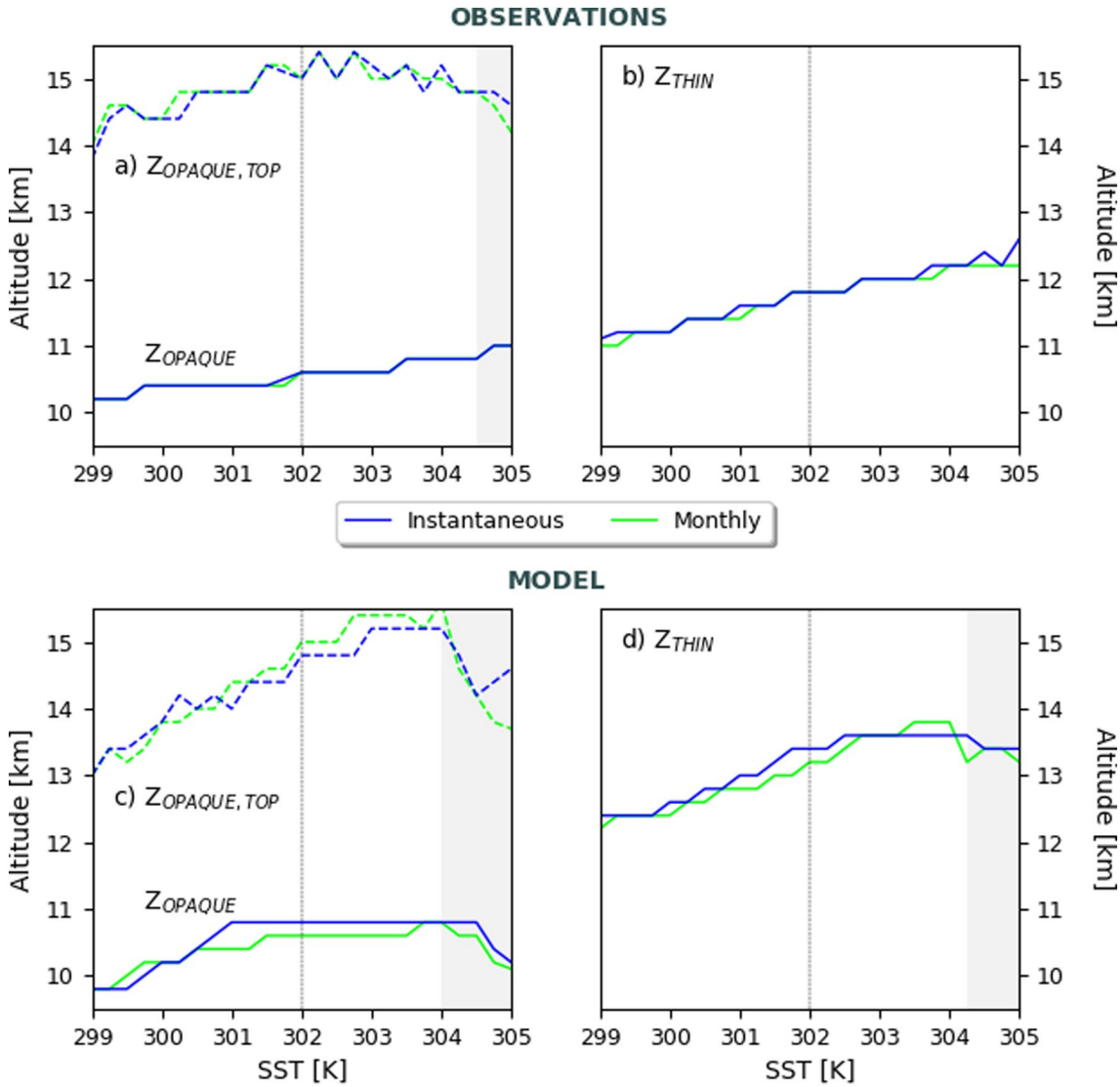

Figure 9. Same as Figure 6, but for the cloud altitudes Z_{OPAQUE}, $Z_{OPAQUE,TOP}$, and Z_{THIN}.

UTRH is of the same sign as the local variation for SSTs between 299 and 302.5 K, where UTRH slightly increases by +0.4%/K (zoom in Figure 11c). Increased UTRH is likely either due to dissipating high clouds, or advection by the large-scale circulation (Pierrhumbert & Roca, 1998; Slingo & Webb, 1997). Previous observational studies have found no significant trends in large-scale UTRH over ocean surfaces in clear-sky situations (Bates & Jackson, 2001; Shi & Bates, 2011), while we consider tropical high cloud situations.

Local instantaneous observations (Figure 11, top panel, blue lines) show constant LTRH over SSTs <302.5 K, whilst increasing MTRH (+8%/K, Figure 11b) as expected from an increase in convective activity over these SSTs (Figure S2g in Supporting Information S1). In contrast, over the warmest SSTs (>303 K), the troposphere dries at all levels, which would increase the outgoing longwave radiation at the top of the atmosphere. The variation of MTRH with SST is consistent with R. H. Johnson and Cielsielski (2013) who found a strong humidification at pressures <500 hPa by vertical transport from DC.

The sensitivity of the RH profile to SST is little affected by what type of high cloud (thin or opaque) is present, as shown by comparison between the instantaneous variations of the RH profile in only grid boxes containing high opaque clouds (dotted blue curve) and any high cloud (solid blue curve) in Figure 11.

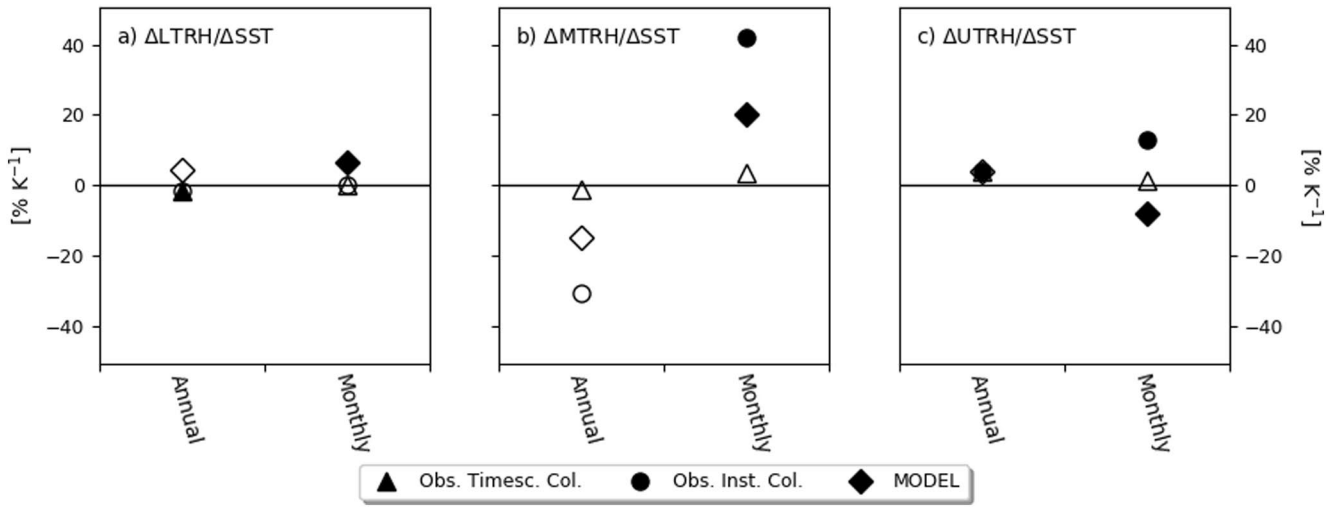

Figure 10. Same as Figure 5, but for $\Delta RH_x/\Delta SST$. (a) LTRH, (b) MTRH, (c) UTRH.

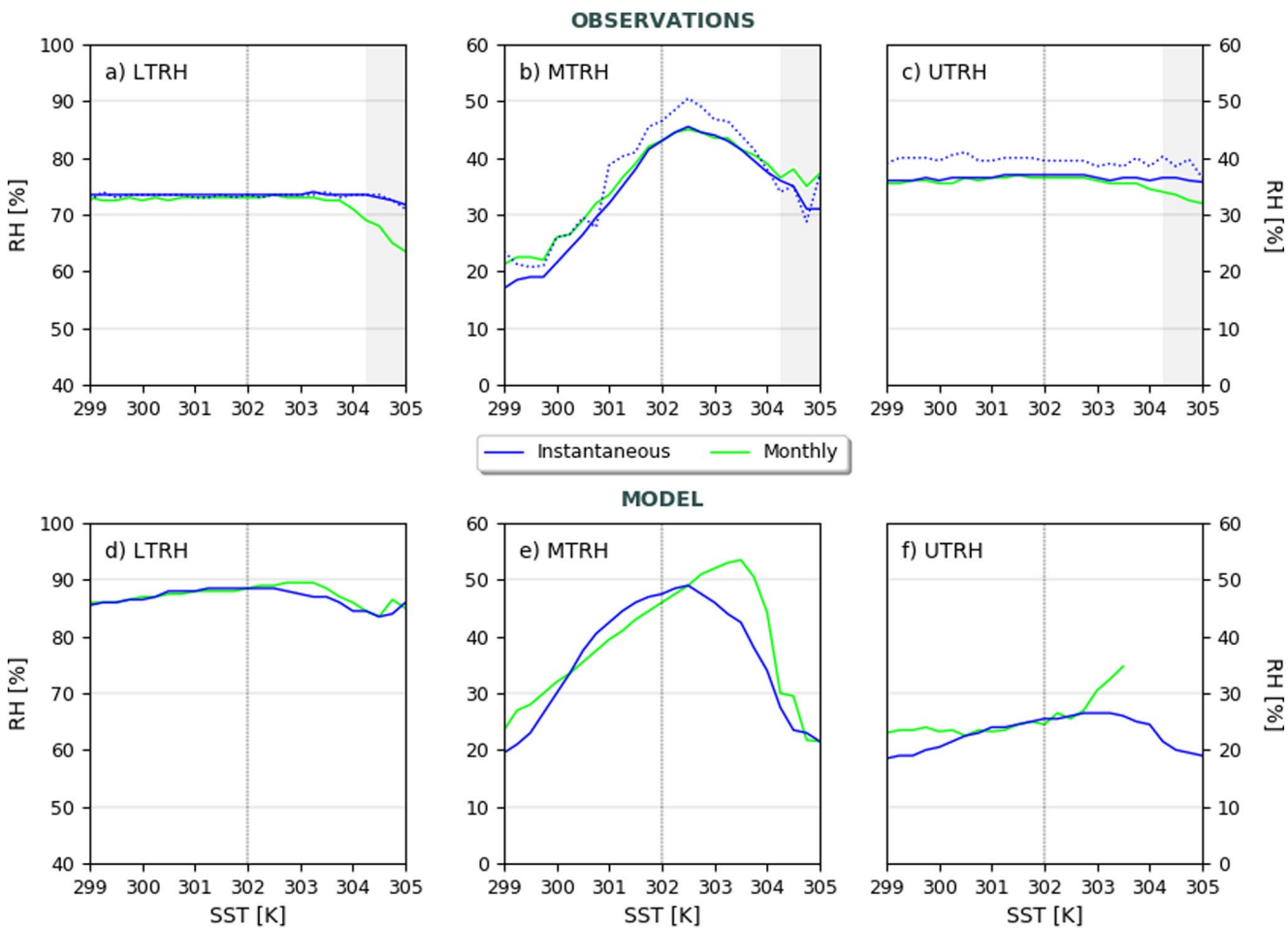

Figure 11. Same as Figure 6, but for LTRH, MTRH, and UTRH. Dotted blue curves: instantaneous variations in grid boxes containing opaque clouds.

The weakly positive or mostly constant (+0.4%/K) UTRH with SST (Figure 11c, SST <303 K) is consistent with previous work at pressures <250 hPa, for example, Garot et al. (2017) and Luo et al. (2012).

5.3.2. Model Variations With SST Current Climate

Annual tropical means (Figure 10, lozenges) show only a significant annual regression for UTRH (+4.2%/K), which is slightly greater than the observed values (+3.6%/K). The +4.2%/K increase is consistent with Sherwood et al. (2010) who simulated an ensemble-mean increase of 0 to +4%/K in the tropical upper troposphere (<200 hPa; 15°N–15°S; 18 coupled ocean-atmosphere AR4 models). Moreover, our observed regressions (Figures 10a and 10b) suggest that the model correctly simulates MTRH variations with SST over large-scale oceanic surfaces, but not annual LTRH which shows a non-significant increase where the Timescale Collocated Method shows a significant decrease.

Local instantaneous simulations (Figure 11, bottom panel) show that the model reproduces the observed sensitivity of LTRH and MTRH to SST quite well. Although, LTRH is overestimated by more than 10%; MTRH peaks at slightly too warm SSTs (+1 K) and decreases too rapidly. Modeled sensitivity of UTRH to SST is less well reproduced, as it is almost constant in the observations. Also, modeled UTRH is underestimated by typically 10% over all SSTs.

5.3.3. Predicted Changes in a Warmer Climate

Figure 7 shows tropical increases in UTRH (+9%, Figure 7g) and MTRH (+8%, Figure 7h) in the AMIP + 4 K scenario. The +8% increase in MTRH (+2%/K) is consistent with Sherwood et al. (2010) who simulated a +3% ensemble-mean increase in equatorial MTRH (500 hPa; 15°N–15°S) for a forced +2 K warming (+1.5%/K). The +9% tropical net increase in UTRH attributed to the +4 K warming is smaller but comparable to the simulated annual mean regressions in the current climate (+4.2 vs. +2.3%/K, Figure 10c).

Because (a) the tropical mean MTRH increases with SST in the observations of current climate (Figure 10b), the modeled current climate (Figure 10b), and in the model response to forced change (Figure 7h), and (b) the local modeled variations of MTRH with SST (Figure 11e) are consistent with the observations (Figure 11b), we are confident that the model simulates the correct sign of MTRH response to a forced change, but not the magnitude. However, we have little confidence in the predicted response of UTRH to forced change, due to the disagreement between modeled and observed sensitivities of UTRH in current climate on both the local and tropical mean scales.

6. Discussion

So far, cloud properties and RH variations with SST have been studied independently. Here, we will analyze them together. Hereafter we exclusively discuss significant variations ($p \leq 0.05$). We discuss those variations considering the Iris, FAT, PHAT, and Stability Iris hypotheses.

6.1. Variations of RH and Clouds With SST

1. On the local scale (Figures 6, 9 and 11), we see signatures of distinct mechanisms

The observed variations of MTRH, C_{OPAQUE}, and $Z_{\mathrm{OPAQUE,TOP}}$ are driven by DC. Indeed, these three variables all increase together (MTRH + 8%/K, C_{OPAQUE} + 11.7%/K, $Z_{\mathrm{OPAQUE,TOP}}$ + 0.3 km/K) after the onset of DC (SST > 299 K), peak at SST ≈302 K and decrease over SST >302 K. This deep convective behavior is quite well reproduced in the model where MTRH, C_{OPAQUE}, $Z_{\mathrm{OPAQUE,TOP}}$ peak together at the same SST, although at SST = 303 K instead of SST = 302 K. Only Z_{OPAQUE} rises monotonically in the observation, whilst peaks in the model.

Observed UTRH and thin clouds are not influenced by DC. UTRH is weakly increasing over SSTs <302 K and decreasing over SSTs >302 K, C_{THIN} is weakly sensitive to SST with a small minimum at SST = 302 K, and Z_{THIN} increases monotonically with SST (+0.21 km/K). The model does not reproduce this observed picture; rather modeled UTRH and C_{THIN} behave similarly to MTRH and C_{OPAQUE}, as if also under the influence of DC.

Z_{OPAQUE} and Z_{THIN} robustly increase with SST on all time and space scales, and are therefore likely more rooted to SST than other variables, and possibly less dependent on the mechanism responsible for creating the high clouds (DC or not).

2. From these local-scale results (Figures 6, 9, and 11), we can get more insight into the annual tropical mean scale results (Figures 5, 8, and 10)

On the annual tropical mean scale, we observe significantly decreasing C_{OPAQUE} (−7.5%/K). Local observations (Figure 6a) suggest that this is a signature of SSTs >302 K, representing half of the high opaque cloud population (52%; Figure S2a in Supporting Information S1), that we find in DC regions.

On the annual tropical mean scale, we also observe significantly decreasing C_{THIN} with SST (−2.6%/K). Local observations suggest that this is a signature of situations over SSTs <302 K, which represent half of the high thin cloud population (51%; Figure 2d). Consistently with observations, the model simulates significantly decreasing C_{THIN} with SST (−2.4%/K) on the annual tropical mean scale, but not for the good reasons because local simulations indicate that the model behavior comes from regions where SSTs >303 K, because the model high clouds mostly come from the large-scale parameterization, contrarily to the observation.

On the annual tropical mean scale, we also observe rising Z_{OPAQUE} (+0.43 km/K) and Z_{THIN} (+0.34 km/K) with SST. These rise-ups are consistent with local observations showing that Z_{OPAQUE} and Z_{THIN} increase monotonically with SST, although at smaller rates. The model also rises Z_{OPAQUE} (+0.56 km/K) and Z_{THIN} (+0.58 km/K) with SST, although slightly too much. Contrarily to other variables, there is an overall agreement on all scales and in both observations and model for rising cloud altitudes with SST.

3. Link with warmer climate

Our comparisons between current climate variability and +4 K warming (Sections.5.1c, 5.2c, 5.3c) showed that the former is more sensitive than the latter to 1 K SST increase for high cloud covers (∼10 times) and UTRH (∼3 times), but close for the cloud altitude and temperature responses. The higher sensitivity of cloud cover has already been documented (e.g., Vaillant de Guélis et al., 2018). Based on our results, rising high cloud altitudes, and increasing MTRH are the most robust water cycle responses to increased SST as observations and model show this, on all time and space scales, in current climate and in the model response to a forced SST increase.

6.2. Sensitivity Study

6.2.1. Diurnal Variation

Our results are presented for daytime data only (01:30 p.m.), but we also analyzed nighttime data around 01:30 a.m. (not shown) and found variations with SST similar to daytime. Slight differences show that, during night, clouds tend to be higher and colder, and smaller over SSTs <303 K, consistently with previous work (e.g., Chepfer et al., 2019; Noel et al., 2018).

6.2.2. Sensitivity to the Definition of the Cloud Cover

Figure 6 shows the median C_{OPAQUE} values in 1° × 1° grid boxes where SST ≥299 K and $T_{Z_{OPAQUE}}$ ≤240 K. We built the same figure (Figure S7 in Supporting Information S1) but using the mean opaque *cloud fraction* CF_{OPAQUE} defined as the sum of only high C_{OPAQUE} (SST ≥ 299 K and $T_{Z_{OPAQUE}} \leq 240$ K) in each 0.25 K SST bin divided by the total number of grid boxes within that 0.25 K SST bin. The results exhibit similar variations with SST on the process scale for the two definitions (CF_{OPAQUE}, C_{OPAQUE}), although CF_{OPAQUE} is shifted to smaller values because most grid boxes in its data set do not contain opaque high clouds. Hence, the *shape* of the variation with SST is independent of definition.

In contrast, the *thin cloud fraction* CF_{THIN} peaks around SST = 303 K (not shown) where C_{THIN} is minimum (Figure 6). This indicates that grid boxes containing no high clouds (but clear or low cloud) are more numerous far away from SST = 302 K.

6.2.3. Sensitivity to Region

We also examined cloud-RH-SST relationships (Figures 5–11) in five independent tropical oceanic regions previously defined in Bouniol et al., 2016; Brown and Kummerow, 2014, Wall and Hartmann, 2018.

On the process scale, the results are similar in all regions and comparable to the all-tropics results, with minor differences (Figures S8–S10 in Supporting Information S1). This result suggests that the processes associated to high clouds are weakly region-dependent, and indicates that the data set (SST $\geq$ 299 K, $T \leq$ 240 K) used in this study show the same observed cloud-RH-SST relationships in each independent tropical oceanic region.

6.3. Implications

6.3.1. FAT and PHAT Hypotheses

Because the FAT/PHAT hypotheses are formulated around statistical equilibrium between convective heating and clear-sky radiative cooling and relates to the global scale, we look for signatures of this mechanism in the opaque cloud tropical mean results. We observe rising opaque cloud altitudes (Figure 8) without significantly varying opaque cloud temperatures (Figure S3 in Supporting Information S1) on the annual tropical mean scale, supporting the FAT (Hartmann & Larson, 2002) hypothesis. Unsurprisingly the model opaque cloud temperature is also consistent with the FAT on the tropical mean scale (Figure S3 in Supporting Information S1).

6.3.2. Iris and Stability Iris Hypotheses

Because the anvil-associated thin clouds cannot be distinguished from the non-convective thin clouds, we cannot say whether the thin cloud property variations are related to DC or not. Hence, we use only the opaque clouds and not thin clouds to evaluate these hypotheses.

On the tropical mean scale, C_{OPAQUE} decreases with warming in the observations, consistent with the Iris hypothesis (Lindzen et al., 2001). In addition, the simultaneous decrease in high cloud cover and rising cloud altitudes are consistent with the Stability Iris mechanism (Bony et al., 2016). On the local scale, the high cloud cover shrinkage with SST is observed for opaque clouds and only over SSTs >302 K. Consequently, these local observations support the Iris and Stability Iris hypotheses over SSTs >302 K for opaque clouds. This observed signature shows up when examining all the tropical oceans combined (Figure 6), and when examining each individual tropical region (Figure S8 in Supporting Information S1), although C_{OPAQUE} peaks at slightly different SST values in each region.

The model disagrees with the Stability Iris hypothesis on the annual tropical mean scale, where it does not reproduce the observed decrease in tropical mean C_{OPAQUE}, but agrees with the Stability Iris hypothesis on the local scale over SSTs >303 K where C_{OPAQUE} decreases.

7. Conclusions

We have analyzed spaceborne observations and model simulations of clouds and RH in tropical high cloud situations (SST $\geq$ 299 K, Cover > 0%, $T \leq$ 240 K) to identify signatures of variations with SST on the process scale and the annual tropical mean scale.

The process scale is represented by median variations with SST on the instantaneous grid box scale. On the process scale, observed middle-tropospheric RH (MTRH), high opaque cloud cover (C_{OPAQUE}), and opaque cloud top altitude ($Z_{\mathrm{OPAQUE,TOP}}$), are driven by DC and covary nonlinearly with SST. Over SSTs 299–302 K, by the onset of DC, C_{OPAQUE} and the opaque cloud altitude of full lidar attenuation (Z_{OPAQUE}) increase with SST and are associated to a considerable pick-up of MTRH there. Over SSTs >302 K, MTRH decreases, C_{OPAQUE} shrinks, and Z_{OPAQUE} continues to rise with SST. In contrast, observed variations of high thin cloud cover (C_{THIN}) and UTRH with SST are much less sensitive to SST. The variation of C_{THIN} complements that of high C_{OPAQUE}, which indicates an anvil optical thickening over SSTs <302 K, whilst an optical thinning over SSTs >302 K, accompanied by a slight drying of UTRH. The thin cloud emission altitude (Z_{THIN}) increases monotonically with SST over 299–305 K. Similar conclusions arise when examining atmospheric situations containing high clouds over all tropical oceans combined and in independent tropical regions. These results are thus independent of tropical region.

When averaged over large areas, high cloud properties and RH vary linearly with SST, so the signatures of cloud mechanisms identified on the process scale are typically smaller or no longer visible. On the tropical mean scale, we observe decreasing high opaque and thin cloud covers and rising altitudes without significant changes in cloud temperature. Area-averaged behaviors roughly correspond to the process observations weighted by the SST distribution. As a result, tropical means are always dominated by one population and mask others. The dominating population is not always the most numerous, but sometimes the one most sensitive to SST change. This is likely why previous observational studies searching for linear co-variations using different spatial and temporal scales, considering different subsamples, or focusing on different areas, reported different conclusions. For example, the decrease in tropical mean C_{OPAQUE} with SST seems to represent the behavior of the local data over SSTs >302 K but masks the behavior of the more numerous opaque clouds over SSTs between 299 and 302 K. In contrast, the decrease in annual tropical mean C_{THIN} (Figure 5b) seems to represent the behavior of most of the local high cloud population over SSTs between 299 and 302 K, and not the behavior over SSTs >302 K that we associate with convective detrainment on the process scale. Contrarily to these complex variations of the cloud covers with SST, the altitudes of opaque and thin high clouds (Z_{OPAQUE}, Z_{THIN}) robustly increase with SST on all time and space scales, suggesting those altitude variations are tied to SST, whatever the high cloud type and cloud origin.

In the model, high opaque and thin clouds exhibit similar sensitivities to SST, as if both were driven by the same mechanism. But the observations show that this is not the case. The model does fairly well with C_{OPAQUE} and MTRH that are both tied to DC but fails to reproduce observed variations of C_{THIN} and UTRH with SST which are not directly tied to DC. Consequently, the model does not capture the variations of the balance between high opaque and thin cloud covers with SST.

Moreover, our results suggest that the signs (not magnitudes) of predicted changes in MTRH and opaque and thin cloud altitudes ($Z_{OPAQUE,}$ Z_{THIN}) as climate warms are quite reliable, whilst the predicted change of the cloud covers (C_{OPAQUE}, C_{THIN}) and UTRH are not. Indeed, the increases of cloud altitudes ($Z_{OPAQUE,}$ Z_{THIN}) and MTRH with SST show up consistently and robustly on all time and space scales in both the model and observations.

As previously shown (Cesana & Chepfer, 2012; Guzman et al., 2017; Stubenrauch et al., 2019), the model fails to reproduce the observed behavior of C_{THIN}. Due to their different responses to SST variations, and to their different interactions with radiation and implications for weather and climate, our observations confirm that more attention should be paid to the evolution of the balance between opaque and thin high clouds with SST (Gasparini et al., 2019, 2021; Hartmann & Berry, 2017; Hartmann et al., 2001) on various time scales from instantaneous to diurnal, decadal and climate.

Data Availability Statement

GOCCP data (Guzman et al., 2017; Vaillant de Guélis et al., 2017) is available through CFMIP-OBS (https://climserv.ipsl.polytechnique.fr/cfmip-obs/), and SAPHIR data (Brogniez et al., 2016) through the Aeris/ICARE ground segment of Megha-Tropiques (https://www.icare.univ-lille.fr/product-documentation/?product=SAPHIR-L2B-RH).

Acknowledgments
The authors thank NASA and CNES for data accessibility, and CNES for its financial support through the EECLAT and Megha-Tropiques projects. The authors thank the national Aeris data center that hosts the satellite data, and the computing resources of ESPRI/IPSL were greatly appreciated. The authors thank Patrick Raberanto (LMD/IPSL), Christophe Dufour (LATMOS/IPSL), and Artem Feofilov (LMD/IPSL) for the gridded GOCCP, SAPHIR L2B, and model data sets, and Marine Bonnazzola (LMD/IPSL) for her valuable inputs. Data sets are available upon request (ESPRI/IPSL Data Center). The authors thank the three anonymous reviewers who helped us to significantly improve the manuscript.

References

Ackerley, D., Chadwick, R., Dommenget, D., & Petrelli, P. (2018). An ensemble of AMIP simulations with prescribed land surface temperatures. *Geoscientific Model Development*, *11*, 3865–3881. https://doi.org/10.5194/gmd-11-3865-2018

Aumann, H. H., Ruzmaikin, A., & Behrangi, A. (2017). Increase in the frequency of tropical deep convective clouds with global warming. *Atmospheric Chemistry and Physics Discussions*. https://doi.org/10.5194/acp-2017-135

Bates, J. J., & Jackson, D. L. (2001). Trends in upper-tropospheric humidity. *Geophysical Research Letters*, *28*, 1695–1698. https://doi.org/10.1029/2000gl012544

Behrangi, A., Kubar, T., & Lambrigtsen, B. (2012). Phenomelogical description of tropical clouds using *CloudSat* cloud classification. *Monthly Weather Review*, *140*, 3235–3249. https://doi.org/10.1175/mwr-d-11-00247.1

Bellenger, H., & Duvel, J.-P. (2009). An analysis of tropical ocean diurnal warm layers. *Journal of Climate*, *22*, 3629–3646. https://doi.org/10.1175/2008JCLI2598.1

Bodas-Salcedo, A., Webb, M. J., Bony, S., Chepfer, H., Dufresne, J.-L., Klein, S. A., et al. (2011). COSP: Satellite simulation software for model assessment. *Bulletin of the American Meteorological Society*, *92*, 1023–1043. https://doi.org/10.1175/2011BAMS2856.1

Boggs, P. T., Byrd, R. H., Rogers, J. E., & Schnabel, R. B. (1992). *User's Reference Guide for ODRPACK Version 2.01 Software for Weighted Orthogonal Distance Regression. Applied and Computational Mathematics Division, Center for Computing and Applied Mathematics Laboratory* (Vol. 4834). NISTIR.

Boggs, P. T., & Rogers, J. E. (1990). *Orthogonal Distance Regression. Applied and Computational Mathematics Division, Center for Computing and Applied Mathematics* (Vol. 89–4197). NISTIR.

Boggs, P. T., Spiegelman, C. H., Donaldson, J. R., & Schnabel, R. B. (1988). A computational examination of orthogonal distance regression. *Journal of Econometrics*, *38*, 169–201. https://doi.org/10.1016/0304-4076(88)90032-2

Bony, S., Stevens, B., Coppin, D., Becker, T., Reed, K. A., Voigt, A., & Medeiros, B. (2016). Thermodynamic control of anvil cloud amount. *Proceedings of the National Academy of Sciences*, *113*, 8927–8932. https://doi.org/10.1073/pnas.1601472113

Bouniol, D., Roca, R., Fiolleau, T., & Poan, D. E. (2016). Macrophysical, microphysical, and radiative properties of tropical mesoscale convective systems over their life cycle. *Journal of Climate*, *29*, 3353–3371. https://doi.org/10.1175/JCLI-D-15-0551.1

Brogniez, H., Fallourd, R., Mallet, C., Sivira, R., & Dufour, C. (2016). Estimating confidence intervals around relative humidity profiles from satellite observations: Applications to the SAPHIR sounder. *Journal of Atmospheric and Oceanic Technology*, *33*, 1005–1022. https://doi.org/10.1175/jtech-d-15-0237.1

Brogniez, H., Kirstetter, P.-E., & Eymard, L. (2013). Expected improvements in the atmospheric humidity profile retrieval using the Megha-Tropiques microwave payload. *Quarterly Journal of the Royal Meteorological Society*, *139*, 842–851. https://doi.org/10.1002/qj.1869

Brown, P. J., & Kummerow, C. D. (2014). An assessment of atmospheric water budget components over tropical oceans. *Journal of Climate*, *27*, 2054–2071. https://doi.org/10.1175/JCLI-D-13-00385.1

Caldwell, P. M., Zelinka, M. D., Taylor, K. E., & Marvel, K. (2016). Quantifying the sources of intermodel spread in equilibrium climate sensitivity. *Journal of Climate*, *29*, 513–524. https://doi.org/10.1175/JCLI-D-15-0352.1

Ceppi, P., Brient, F., Zelinka, M. D., & Hartmann, D. L. (2017). Cloud feedback mechanisms and their representation in global climate models. *WIREs Climate Change*, *8*(4), e465. https://doi.org/10.1002/wcc.465

Ceppi, P., & Gregory, J. M. (2017). Relationship of tropospheric stability to climate sensitivity and Earth's observed radiation budget. *Proceedings of the National Academy of Sciences*, *14*, 13126–13131. https://doi.org/10.1073/pnas.1714308114

Cesana, G., & Chepfer, H. (2012). How well do climate models simulate cloud vertical structure? A comparison between CALIPSO-GOCCP satellite observations and CMIP5 models. *Geophysical Research Letters*, *39*, L20803. https://doi.org/10.1029/2012GL053153

Chepfer, H., Bony, S., Winker, D., Cesana, G., Dufresne, J. L., Minnis, P., et al. (2010). The GCM-Oriented CALIPSO Cloud Product (CALIPSO-GOCCP). *Journal of Geophysical Research*, *115*, 1–13. https://doi.org/10.1029/2009jd012251

Chepfer, H., Bony, S., Winker, D., Chiriaco, M., Dufresne, J.-L., & Seze, G. (2008). Use of CALIPSO lidar observations to evaluate the cloudiness simulated by a climate model. *Geophysical Research Letters*, *35*, L15704. https://doi.org/10.1029/2008GL034207

Chepfer, H., Brogniez, H., & Noel, V. (2019). Diurnal variations of cloud and relative humidity profiles across the tropics. *Nature Scientific Reports*, *9*, 16045. https://doi.org/10.1038/s41598-019-52437-6

Chepfer, H., Noel, V., Winker, D., & Chiriaco, M. (2014). Where and when will we observe cloud changes due to climate warming? *Geophysical Research Letters*, *41*, 8387–8395. https://doi.org/10.1002/2014GL061792

Choi, Y.-S., Kim, W., Yeh, S.-W., Masunaga, H., Kwon, M.-J., Jo, H.-S., & Huang, L. (2017). Revisiting the Iris effect of tropical cirrus clouds with TRMM and A-Train satellite data. *Journal of Geophysical Research: Atmospheres*, *122*, 5917–5931. https://doi.org/10.1002/2016JD025827

Dee, D. P., Uppala, S. M., Simmons, A. J., Berrisford, P., Poli, P., Kobayashi, S., et al. (2011). The ERA-Interim reanalysis: Configuration and performance of the data assimilation system. *Quarterly Journal of the Royal Meteorological Society*, *137*, 553–597. https://doi.org/10.1002/qj.828

Del Genio, A. D., & Kovari, W. (2002). Climatic properties of tropical precipitating convection under varying environmental conditions. *Journal of Climate*, *15*, 2597–2615. https://doi.org/10.1175/1520-0442(2002)015<2597:cpotpc>2.0.co;2

Dessler, A. E. (2010). A determination of the cloud feedback from climate variations over the past decade. *Science*, *330*, 1523–1527. https://doi.org/10.1126/science.1192546

Eitzen, Z. A., Xu, K.-M., & Wong, T. (2009). Cloud and radiative characteristics of tropical deep convective systems in extended cloud objects from CERES observations. *Journal of Climate*, *22*, 5983–6000. https://doi.org/10.1175/2009JCLI3038.1

Evans, J. L., & Webster, C. C. (2014). A variable sea surface temperature threshold for tropical convection. *Australian Meteorological and Oceanographic Journal*, *64*, S1–S8. https://doi.org/10.22499/2.6401.007

Eymard, L., Gheudin, M., Laborie, P., Sirou, F., Le Gac, C., Vinson, J. P., et al. (2002). The SAPHIR humidity sounder. *Notes Activities Instrumental de l'IPSL*, *24*

Fisher, R. A. (1956). *Statistical methods and scientific inference*. Hafner.

Forster, P. M., Richardson, T., Maycock, A. C., Smith, C. J., Samset, B. H., Myhre, G., et al. (2016). Recommendations for diagnosing effective radiative forcing from climate models for CMIP6. *Journal of Geophysical Research: Atmospheres*, *121*, 12460–12475. https://doi.org/10.1002/2016JD025320

Garot, T., Brogniez, H., Fallourd, R., & Viltard, N. (2017). Evolution of the distribution of upper-tropospheric humidity over the Indian Ocean: Connection with large-scale advection and local cloudiness. *Journal of Applied Meteorology and Climatology*, *56*, 2035–2052. https://doi.org/10.1175/JAMC-D-16-0193.1

Gasparini, B., Blossey, P. N., Hartmann, D. L., Lin, G., & Fan, J. (2019). What drives the life cycle of tropical anvil clouds? *Journal of Advances in Modeling Earth Systems*, *11*, 2586–2605. https://doi.org/10.1029/2019MS001736

Gasparini, B., Rasch, P. J., Hartmann, D. L., Wall, C. J., & Dutsch, M. (2021). A Lagrangian perspective on tropical anvil cloud lifecycle in present and future climate. *Journal of Geophysical Research: Atmospheres*, *126*, e2020JD033487. https://doi.org/10.1029/2020JD033487

Guzman, R., Chepfer, H., Noel, V., Vaillant de Guélis, T., Kay, J. E., Raberanto, P., et al. (2017). Direct atmosphere opacity observations from CALIPSO provide new constraints on cloud-radiation interactions. *Journal of Geophysical Research: Atmospheres*, *122*, 1066–1085. https://doi.org/10.1002/2016jd025946

Hartmann, D. L., & Berry, S. E. (2017). The balanced radiative effect of tropical anvil clouds. *Journal of Geophysical Research: Atmospheres*, *122*, 5003–5020. https://doi.org/10.1002/2017JD026460

Hartmann, D. L., & Larson, K. (2002). An important constraint on tropical cloud—Climate feedback. *Geophysical Research Letters*, *29*, 12-1–12-4. https://doi.org/10.1029/2002GL015835

Hartmann, D. L., & Michelsen, M. L. (2002). No evidence for Iris. *Bulletin of American Meteorological Society*, *83*, 249–254. https://doi.org/10.1175/1520-0477(2002)083<0249:nefi>2.3.co;2

Hartmann, D. L., Moy, L. A., & Fu, Q. (2001). Tropical convection and the energy balance at the top of the atmosphere. *Journal of Climate*, *14*(24), 4495–4511. https://doi.org/10.1175/1520-0442(2001)014<4495:tcateb>2.0.co;2

Hoffmann, L., Günther, G., Li, D., Stein, O., Wu, X., Griessbach, S., et al. (2018). From ERA-Interim to ERA5: Considerable impact of ECMWF's next-generation reanalysis on Lagrangian transport simulations. *Atmospheric Chemistry and Physics*, 1–38. https://doi.org/10.5194/acp-2018-1199

Höjgård-Olsen, E., Brogniez, H., & Chepfer, H. (2020). Observed evolution of the tropical atmospheric water cycle with sea surface temperature. *Journal of Climate*, *33*, 3449–3470. https://doi.org/10.1175/JCLI-D-19-0468.1

Hourdin, F., Musat, I., Bony, S., Braconnot, P., Codron, F., Dufresne, J.-L., et al. (2006). The LMDZ4 general circulation model: Climate performance and sensitivity to parameterized physics with emphasis on tropical convection. *Climate Dynamics*, *27*, 787–813. https://doi.org/10.1007/s00382-006-0158-0

Hourdin, F., Rio, C., Grandpeix, J.-Y., Madeleine, J.-B., Cheruy, F., Rochetin, N., et al. (2020). LMDZ6A: The atmospheric component of the IPSL climate model with improved and better tuned physics. *Journal of Advances in Modeling Earth Systems*, *12*, e2019MS001892. https://doi.org/10.1029/2019MS001892

Houze, R. A., Rasmussen, K. L., Zuluaga, M. D., & Brodzik, S. R. (2015). The variable nature of convection in the tropics and subtropics: A legacy of 16 yr of the tropical rainfall measuring mission satellite. *Reviews of Geophysics*, *53*, 994–1021. https://doi.org/10.1002/2015rg000488

Hughes, K. G., Moum, J. N., & Shroyer, E. L. (2020). Evolution of the velocity structure in the diurnal warm layer. *Journal of Physical Oceanography*, *50*, 617–631. https://doi.org/10.1175/JPO-D-19-0207.1

Igel, M. R., Drager, A. J., & van den Heever, S. C. (2014). A CloudSat cloud object partitioning technique and assessment and integration of deep convective anvil sensitivities to sea surface temperature. *Journal of Geophysical Research: Atmospheres*, *119*, 10515–10535. https://doi.org/10.1002/2014JD021717

Johnson, N. C., & Xie, S.-P. (2010). Changes in the sea surface temperature threshold for tropical convection. *Nature Geoscience*, *3*, 842–845. https://doi.org/10.1038/ngeo1008

Johnson, R. H., & Cielsielski, P. E. (2013). Structure and properties of Madden-Julian oscillations deduces from DYNAMO sounding arrays. *Journal of the Atmospheric Sciences*, *70*, 3157–3179. https://doi.org/10.1175/JAS-D-13-065.1

Klein, S. A., Hall, A., Norris, J. R., & Pincus, R. (2017). Low-cloud feedbacks from cloud controlling factors: A review. *Survey of Geophysics*, *38*, 1307–1329. https://doi.org/10.1007/s10712-017-9433-3

Kuang, Z., & Hartmann, D. L. (2007). Testing the fixed anvil temperature hypothesis in a cloud-resolving model. *Journal of Climate*, *20*, 2051–2057. https://doi.org/10.1175/JCLI4124.1

Leng, L., Zhang, T., Kleinman, L., & Zhu, W. (2007). Ordinary least squares regression, orthogonal distance regression, geometric mean regression and their applications in aerosol science. *Journal of Physics: Conference Series*, *78*, 012084. https://doi.org/10.1088/1742-6596/78/1/012084

Li, R. L., Storelvmo, T., Fedorov, A. V., & Choi, Y.-S. (2019). A positive Iris feedback: Insights from climate simulations with temperature-sensitive cloud-rain conversion. *Journal of Climate*, *32*, 5305–5324. https://doi.org/10.1175/JCLI-D-18-0845.1

Li, Y., Yang, P., North, G. R., & Dessler, A. (2012). Test of the fixed anvil temperature hypothesis. *Journal of the Atmospheric Sciences*, *69*, 2317–2328. https://doi.org/10.1175/JAS-D-11-0158.1

Lin, B., Wielicki, B., Chambers, L. H., Hu, Y., & Xu, K.-M. (2002). The Iris hypothesis: A negative or positive cloud feedback? *Journal of Climate*, *15*, 3–7. https://doi.org/10.1175/1520-0442(2002)015<0003:tihano>2.0.co;2

Lin, B., Wong, T., Wielicki, B., & Hu, Y. (2004). Examination of the decadal tropical mean *ERBS* nonscanner radiation data for the Iris hypothesis. *Journal of Climate*, *17*, 1239–1246. https://doi.org/10.1175/1520-0442(2004)017<1239:eotdtm>2.0.co;2

Lindzen, R. S., & Choi, Y.-S. (2021). The Iris effect: A review. *Asia-Pacific Journal of Atmospheric Sciences*, *58*, 159–168. https://doi.org/10.1007/s13143-021-00238-1

Lindzen, R. S., Chou, M.-D., & Hou, A. Y. (2001). Does the Earth have an adaptive infrared Iris? *Bulletin of the American Meteorological Society*, *82*, 417–432. https://doi.org/10.1175/1520-0477(2001)082<0417:dtehaa>2.3.co;2

Lolli, B., & Gasperini, P. (2012). A comparison among general orthogonal regression methods applied to earthquake magnitude conversions. *Geophysical Journal International*, *190*, 1135–1151. https://doi.org/10.1111/j.1365-246X.2012.05530.x

Luo, Z. J., Kley, D., Johnson, R. H., Liu, G. Y., Nawrath, S., & Smit, H. G. J. (2012). Influence of sea surface temperature on humidity and temperature in the outflow of tropical deep convection. *Journal of Climate*, *25*, 1340–1348. https://doi.org/10.1175/2011JCLI4124.1

Luo, Z. J., & Rossow, W. B. (2004). Characterizing tropical cirrus life cycle, evolution, and interaction with upper-tropospheric water vapor using Lagrangian trajectory analysis of satellite observations. *Journal of Climate*, *17*, 4541–4563. https://doi.org/10.1175/3222.1

Mauritsen, T., & Stevens, B. (2015). Missing Iris effect as a possible cause of muted hydrological change and high climate sensitivity in models. *Nature Geoscience*, *8*, 346–351. https://doi.org/10.1038/ngeo2414

Noel, V., Chepfer, C., Chiriaco, M., & Yorks, J. (2018). The diurnal cycle of cloud profiles over land and ocean between 51°S and 51°N, seen by the CATS spaceborne lidar from the International Space Station. *Atmospheric Chemistry and Physics*, *18*, 9457–9473. https://doi.org/10.5194/acp-18-9457-2018

Norris, J. R., Allen, R. J., Evan, A. T., Zelinka, M. D., O'Dell, C. W., & Klein, S. A. (2016). Evidence for climate change in the satellite cloud record. *Nature*, *536*, 72–75. https://doi.org/10.1038/nature18273

Orlanski, I. (1975). A rational subdivision of scales for atmospheric processes. *Bulletin of the American Meteorological Society*, *56*, 527–530.

Perpina, M., Noel, V., Chepfer, H., Guzman, R., & Feofilov, A. (2021). Link between opaque cloud properties and atmospheric dynamics in observations and simulations of current climate in the tropics, and impact on future predictions. *Journal of Geophysical Research: Atmospheres*, *17*, e2020JD033899. https://doi.org/10.1029/2020JD033899

Pierrhumbert, R. T., & Roca, R. (1998). Evidence for control of Atlantic subtropical humidity by large scale advection. *Geophysical Research Letters*, *25*, 4537–4540.

Rapp, A. D., Kummerow, C., Berg, W., & Griffith, B. (2005). An evaluation of the proposed mechanism of the adaptive infrared Iris hypothesis using *TRMM* VIRS and PR measurements. *Journal of Climate*, *18*, 4185–4194. https://doi.org/10.1175/JCLI3528.1

Reverdy, M., Noel, V., Chepfer, H., & Legras, B. (2012). On the origins of subvisible cirrus clouds in the tropical upper troposphere. *Atmospheric Chemistry and Physics*, *12*, 12081–12101. https://doi.org/10.5194/acp-12-12081-2012

Roca, R., Brogniez, H., Chambon, P., Chomette, O., Cloché, S., Gosset, M. E., et al. (2015). The Megha-Tropiques mission: A review after three years in orbit. *Frontiers in Earth Science*, *3*, 1–14. https://doi.org/10.3389/feart.2015.00017

Sabin, T. P., Babu, C. A., & Joseph, P. V. (2013). SST-convection relation over tropical oceans. *International Journal of Climatology*, *33*, 1424–1435. https://doi.org/10.1002/joc.3522

Saint-Lu, M., Bony, S., & Dufresne, J.-L. (2020). Observational evidence for a stability Iris effect in the tropics. *Geophysical Research Letters*, *47*, e2020GL089059. https://doi.org/10.1029/2020GL089059

Seeley, J. T., Jeevanjee, N., & Romps, D. M. (2019). FAT or FiTT: Are anvil clouds or the tropopause temperature invariant? *Geophysical Research Letters*, *46*, 1842–1850. https://doi.org/10.1029/2018GL080096

Sherwood, S. C., Ingram, W., Tsushima, Y., Satoh, M., Roberts, M., Vidale, P. L., & O'Gorman, P. A. (2010). Relative humidity changes in a warmer climate. *Journal of Geophysical Research*, *115*. https://doi.org/10.1029/2009JD012585

Sherwood, S. C., Webb, M. J., Annan, J. D., Armour, K. C., Forster, P. M., Hargreaves, J. C., et al. (2020). An assessment of Earth's climate sensitivity using multiple lines of evidence. *Reviews of Geophysics*, *58*, e2019RG000678. https://doi.org/10.1029/2019RG000678

Shi, L., & Bates, J. J. (2011). Three decades of intersatellite-calibrated high-resolution infrared radiation sounder upper tropospheric water vapor. *Journal of Geophysical Research*, *116*. https://doi.org/10.1029/2010JD014847

Sivira, R. G., Brogniez, H., Mallet, C., & Oussar, Y. (2015). A layer-average relative humidity profile retrieval for microwave observations: Design and results for the Megha-Tropiques payload. *Atmospheric Measurement Techniques*, *8*, 1055–1071. https://doi.org/10.5194/amt-8-1055-2015

Slingo, A., & Webb, M. J. (1997). The spectral signature of global warming. *Quarterly Journal of the Royal Meteorological Society*, *123*, 293–307. https://doi.org/10.1002/qj.49712353803

Steyn, D. G., Oke, T. R., Hay, J. E., & Knox, J. L. (1981). On the scales in meteorology and climate. *Climatological Bulletin*, *39*, 1–8.

Stubenrauch, C. J., Bonazzola, M., Protopapadaki, S. E., & Musat, I. (2019). New cloud system metrics to assess bulk ice cloud schemes in a GCM. *Journal of Advances in Modeling Earth Systems*, *11*, 3212–3234. https://doi.org/10.1029/2019MS001642

Su, H., Jiang, J. H., Gu, Y., Neelin, J. D., Kahn, B. H., Feldman, D., et al. (2008). Variations of tropical upper tropospheric clouds with sea surface temperature and implications of radiative effects. *Journal of Geophysical Research*, *113*, 1–13. https://doi.org/10.1029/2007jd009624

Su, H., Jiang, J. H., Gu, Y., Neelin, J. D., Shen, T. J., Zhai, C., et al. (2017). Tightening of tropical ascent and high clouds key to precipitation change in a warmer climate. *Nature Communications*, *8*, 1–9. https://doi.org/10.1038/ncomms15771

Swales, D. J., Pincus, R., & Bodas-Salcedo, A. (2018). The Cloud Feedback Model Intercomparison Project Observational Simulator Package: Version 2 (COSP2). *Geophysical Model Developments*, *11*, 77–81. https://doi.org/10.5194/gmd-11-77-2018

Thompson, D. W. J., Bony, S., & Li, Y. (2017). Thermodynamic constraint on the depth of the global tropospheric circulation. *Proceedings of the National Academy of Sciences*, *114*, 8181–8186. https://doi.org/10.1073/pnas.1620493114

Vaillant de Guélis, T., Chepfer, H., Guzman, R., Bonazzola, M., Winker, D. M., & Noel, V. (2018). Space lidar observations constrain longwave cloud feedback. *Nature Scientific Reports*, *8*, 16570. https://doi.org/10.1038/s41598-018-34943-1

Vaillant de Guélis, T., Chepfer, H., Noel, V., Guzman, R., Dubuisson, P., Winker, D. M., & Kato, S. (2017). The link between outgoing longwave radiation and the altitude at which a spaceborne lidar beam is fully attenuated. *Atmospheric Measurement Techniques*, *10*, 4659–4685. https://doi.org/10.5194/amt-10-4659-2017

Vial, J., Dufresne, J.-L., & Bony, S. (2013). On the interpretation of inter-model spread in CMIP5 climate sensitivity estimates. *Climate Dynamics*, *41*, 3339–3362. https://doi.org/10.1007/s00382-013-1725-9

Waliser, D. E., Graham, N. E., & Gautier, C. (1993). Comparison of the high reflective cloud and outgoing longwave radiation data sets for use in estimation tropical deep convection. *Journal of Climate*, *6*, 331–353. https://doi.org/10.1175/1520-0442(1993)006<0331:cothrc>2.0.co;2

Wall, C. J., & Hartmann, D. L. (2018). Balanced cloud radiative effects across a range of dynamical conditions over the tropical West Pacific. *Geophysical Research Letters*, *5*, 1–9. https://doi.org/10.1029/2018GL080046

Winker, D. M., Vaughan, M. A., Omar, A., Hu, Y., Powell, K. A., Liu, Z., et al. (2009). Overview of the CALIPSO mission and CALIOP data processing algorithms. *Journal of Atmospheric and Oceanic Technology*, *26*, 2310–2323. https://doi.org/10.1175/2009jtecha1281.1

Xu, K.-M., Wong, T., Wielicki, B. A., Parker, L., Lin, B., Eitzen, Z. A., & Branson, M. (2007). Statistical analyses of satellite cloud object data from CERES. Part II: Tropical convective cloud objects during 1998 El Niño and evidence for supporting the fixed anvil temperature hypothesis. *Journal of Climate*, *20*, 819–842. https://doi.org/10.1175/jcli4069.1

Yoshimori, M., Lambert, F. H., Webb, M. J., & Andrews, T. (2020). Fixed anvil temperature feedback: Positive, zero, or negative? *Journal of Climate*, *33*, 2719–2739. https://doi.org/10.1175/JCLI-D-19-0108.1

Zelinka, M. D., & Hartmann, D. L. (2010). Why is longwave cloud feedback positive? *Journal of Geophysical Research*, *115*. https://doi.org/10.1029/2010JD013817

Zelinka, M. D., & Hartmann, D. L. (2011). The observed sensitivity of high clouds to mean surface temperature anomalies in the tropics. *Journal of Geophysical Research*, *116*. https://doi.org/10.1029/2011JD016459

Zelinka, M. D., Klein, S. A., Taylor, K. E., Andrews, T., Webb, M., Gregory, J. M., & Forster, P. M. (2013). Contributions of different cloud types to feedbacks and rapid adjustments in CMIP5. *Journal of Climate*, *26*, 5007–5027. https://doi.org/10.1175/JCLI-D-12-00555.1

Zelinka, M. D., Myers, T. A., McCoy, D. T., Po-Chedley, S., Caldwell, P. M., Ceppi, P., et al. (2020). Causes of higher climate sensitivity in CMIP6 models. *Geophysical Research Letters*, *47*, e2019GL085782. https://doi.org/10.1029/2019gl085782

Zelinka, M. D., Randall, D. A., Webb, M. J., & Klein, S. A. (2017). Clearing clouds of uncertainty. *Nature Climate Change*, *7*, 674–678. https://doi.org/10.1038/nclimate3402

Zelinka, M. D., Zhou, C., & Klein, S. A. (2016). Insights from a refined decomposition of cloud feedbacks. *Geophysical Research Letters*, *43*, 9259–9269. https://doi.org/10.1002/2016GL069917

Zhou, C., Dessler, A. E., Zelinka, M. D., Yang, P., & Wang, T. (2014). Cirrus feedback on interannual climate fluctuations. *Geophysical Research Letters*, *41*, 9166–9173. https://doi.org/10.1002/2014GL062095

Zhou, C., Zelinka, M. D., Dessler, A. E., & Klein, S. A. (2015). The relationship between interannual and long-term cloud feedbacks. *Geophysical Research Letters*, *42*, 10463–10469. https://doi.org/10.1002/2015GL066698